[21] D. F. Wong, P. B. Rosenberg, Y. Zhou et al., "In vivo imaging of amyloid deposition in Alzheimer disease using the radioligand $^{18}$F-AV-45 (flobetapir F 18)," *Journal of Nuclear Medicine*, vol. 51, no. 6, pp. 913–920, 2010.

[22] M. Koole, D. M. Lewis, C. Buckley et al., "Whole-body biodistribution and radiation dosimetry of $^{18}$F-GE067: a radioligand for in vivo brain amyloid imaging," *Journal of Nuclear Medicine*, vol. 50, no. 5, pp. 818–822, 2009.

[23] M. Ono, M. Haratake, M. Nakayama et al., "Synthesis and biological evaluation of (*E*)-3-styrylpyridine derivatives as amyloid imaging agents for Alzheimer's disease," *Nuclear Medicine and Biology*, vol. 32, no. 4, pp. 329–335, 2005.

[24] W. Qu, M. P. Kung, C. Hou, T. E. Benedum, and H. F. Kung, "Novel styrylpyridines as probes for SPECT imaging of amyloid plaques," *Journal of Medicinal Chemistry*, vol. 50, no. 9, pp. 2157–2165, 2007.

[25] W. Qu, M. P. Kung, C. Hou, L. W. Jin, and H. F. Kung, "Radioiodinated aza-diphenylacetylenes as potential SPECT imaging agents for $\beta$-amyloid plaque detection," *Bioorganic and Medicinal Chemistry Letters*, vol. 17, no. 13, pp. 3581–3584, 2007.

[26] M. P. Kung, C. Hou, Z. P. Zhuang et al., "IMPY: an improved thioflavin-T derivative for in vivo labeling of $\beta$-amyloid plaques," *Brain Research*, vol. 956, no. 2, pp. 202–210, 2002.

[27] Z. P. Zhuang, M. P. Kung, A. Wilson et al., "Structure-activity relationship of imidazo[1,2-a]pyridines as ligands for detecting $\beta$-amyloid plaques in the brain," *Journal of Medicinal Chemistry*, vol. 46, no. 2, pp. 237–243, 2003.

[28] M. P. Kung, C. Hou, Z. P. Zhuang, D. Skovronsky, and H. F. Kung, "Binding of two potential imaging agents targeting amyloid plaques in postmortem brain tissues of patients with Alzheimer's disease," *Brain Research*, vol. 1025, no. 1-2, pp. 98–105, 2004.

[29] Z. P. Zhuang, M. P. Kung, C. Hou et al., "Radioiodinated styrylbenzenes and thioflavins as probes for amyloid aggregates," *Journal of Medicinal Chemistry*, vol. 44, no. 12, pp. 1905–1914, 2001.

[30] Z. P. Zhuang, M. P. Kung, C. Hou et al., "IBOX(2-(4′-dimethylaminophenyl)-6-iodobenzoxazole): a ligand for imaging amyloid plaques in the brain," *Nuclear Medicine and Biology*, vol. 28, no. 8, pp. 887–894, 2001.

[31] M. Ono, M. P. Kung, C. Hou, and H. F. Kung, "Benzofuran derivatives as A$\beta$-aggregate-specific imaging agents for Alzheimer's disease," *Nuclear Medicine and Biology*, vol. 29, no. 6, pp. 633–642, 2002.

[32] H. Watanabe, M. Ono, M. Haratake, N. Kobashi, H. Saji, and M. Nakayama, "Synthesis and characterization of novel phenylindoles as potential probes for imaging of $\beta$-amyloid plaques in the brain," *Bioorganic and Medicinal Chemistry*, vol. 18, no. 13, pp. 4740–4746, 2010.

[33] M. P. Kung, C. Hou, Z. P. Zhuang, A. J. Cross, D. L. Maier, and H. F. Kung, "Characterization of IMPY as a potential imaging agent for $\beta$-amyloid plaques in double transgenic PSAPP mice," *European Journal of Nuclear Medicine and Molecular Imaging*, vol. 31, no. 8, pp. 1136–1145, 2004.

[34] A. B. Newberg, N. A. Wintering, C. M. Clark et al., "Use of $^{123}$I IMPY SPECT to differentiate Alzheimer's disease from controls," *The Journal of Nuclear Medicine*, vol. 47, supplement 1, p. 78P, 2006.

[35] A. B. Newberg, N. A. Wintering, K. Plössl et al., "Safety, biodistribution, and dosimetry of $^{123}$I-IMPY: a novel amyloid plaque-imaging agent for the diagnosis of Alzheimer's disease," *Journal of Nuclear Medicine*, vol. 47, no. 5, pp. 748–754, 2006.

[36] K. Ono, Y. Yoshiike, A. Takashima, K. Hasegawa, H. Naiki, and M. Yamada, "Potent anti-amyloidogenic and fibril-destabilizing effects of polyphenols in vitro: implications for the prevention and therapeutics of Alzheimer's disease," *Journal of Neurochemistry*, vol. 87, no. 1, pp. 172–181, 2003.

[37] M. Ono, N. Yoshida, K. Ishibashi et al., "Radioiodinated flavones for in vivo imaging of $\beta$-amyloid plaques in the brain," *Journal of Medicinal Chemistry*, vol. 48, no. 23, pp. 7253–7260, 2005.

[38] T. Iwatsubo, A. Odaka, N. Suzuki, H. Mizusawa, N. Nukina, and Y. Ihara, "Visualization of A$\beta$42(43) and A$\beta$40 in senile plaques with end-specific A$\beta$ monoclonals: evidence that an initially deposited species is A$\beta$42(43)," *Neuron*, vol. 13, no. 1, pp. 45–53, 1994.

[39] J. C. Morris, M. Storandt, D. W. McKeel et al., "Cerebral amyloid deposition and diffuse plaques in "normal" aging: evidence for presymptomatic and very mild Alzheimer's disease," *Neurology*, vol. 46, no. 3, pp. 707–719, 1996.

[40] H. F. Kung, C. W. Lee, Z. P. Zhuang, M. P. Kung, C. Hou, and K. Plössl, "Novel stilbenes as probes for amyloid plaques," *Journal of the American Chemical Society*, vol. 123, no. 50, pp. 12740–12741, 2001.

[41] M. Ono, M. Haratake, H. Mori, and M. Nakayama, "Novel chalcones as probes for in vivo imaging of $\beta$-amyloid plaques in Alzheimer's brains," *Bioorganic and Medicinal Chemistry*, vol. 15, no. 21, pp. 6802–6809, 2007.

[42] M. Ono, M. Hori, M. Haratake, T. Tomiyama, H. Mori, and M. Nakayama, "Structure-activity relationship of chalcones and related derivatives as ligands for detecting of $\beta$-amyloid plaques in the brain," *Bioorganic and Medicinal Chemistry*, vol. 15, no. 19, pp. 6388–6396, 2007.

[43] M. Ono, M. Haratake, H. Mori, and M. Nakayama, "Novel chalcones as probes for in vivo imaging of $\beta$-amyloid plaques in Alzheimer's brains," *Bioorganic and Medicinal Chemistry*, vol. 15, no. 21, pp. 6802–6809, 2007.

[44] M. Ono, Y. Maya, M. Haratake, K. Ito, H. Mori, and M. Nakayama, "Aurones serve as probes of $\beta$-amyloid plaques in Alzheimer's disease," *Biochemical and Biophysical Research Communications*, vol. 361, no. 1, pp. 116–121, 2007.

[45] Y. Maya, M. Ono, H. Watanabe, M. Haratake, H. Saji, and M. Nakayama, "Novel radioiodinated aurones as probes for SPECT imaging of $\beta$-amyloid plaques in the brain," *Bioconjugate Chemistry*, vol. 20, no. 1, pp. 95–101, 2009.

[46] W. Qu, M. P. Kung, C. Hou, S. Oya, and H. F. Kung, "Quick assembly of 1,4-diphenyltriazoles as probes targeting $\beta$-amyloid aggregates in Alzheimer's disease," *Journal of Medicinal Chemistry*, vol. 50, no. 14, pp. 3380–3387, 2007.

[47] R. Chandra, M. P. Kung, and H. F. Kung, "Design, synthesis, and structure-activity relationship of novel thiophene derivatives for $\beta$-amyloid plaque imaging," *Bioorganic and Medicinal Chemistry Letters*, vol. 16, no. 5, pp. 1350–1352, 2006.

[48] M. Ono, M. Haratake, H. Saji, and M. Nakayama, "Development of novel $\beta$-amyloid probes based on 3,5-diphenyl-1,2,4-oxadiazole," *Bioorganic and Medicinal Chemistry*, vol. 16, no. 14, pp. 6867–6872, 2008.

[49] H. Watanabe, M. Ono, R. Ikeoka, M. Haratake, H. Saji, and M. Nakayama, "Synthesis and biological evaluation of radioiodinated 2,5-diphenyl-1,3,4-oxadiazoles for detecting $\beta$-amyloid plaques in the brain," *Bioorganic and Medicinal Chemistry*, vol. 17, no. 17, pp. 6402–6406, 2009.

[50] H. Han, C. G. Cho, and P. T. Lansbury Jr., "Technetium complexes for the quantitation of brain amyloid," *Journal of the American Chemical Society*, vol. 118, no. 18, pp. 4506–4507, 1996.

[51] N. A. Dezutter, R. J. Dom, T. J. De Groot, G. M. Bormans, and A. M. Verbruggen, "$^{99m}$Tc-MAMA-chrysamine G, a probe for beta-amyloid protein of Alzheimer's disease," *European Journal of Nuclear Medicine*, vol. 26, no. 11, pp. 1392–1399, 1999.

[52] K. Serdons, T. Verduyckt, J. Cleynhens et al., "Synthesis and evaluation of a $^{99m}$Tc-BAT-phenylbenzothiazole conjugate as a potential in vivo tracer for visualization of amyloid $\beta$," *Bioorganic and Medicinal Chemistry Letters*, vol. 17, no. 22, pp. 6086–6090, 2007.

[53] X. Chen, P. Yu, L. Zhang, and B. Liu, "Synthesis and biological evaluation of $^{99m}$Tc, Re-monoamine-monoamide conjugated to 2-(4-aminophenyl)benzothiazole as potential probes for $\beta$-amyloid plaques in the brain," *Bioorganic and Medicinal Chemistry Letters*, vol. 18, no. 4, pp. 1442–1445, 2008.

[54] Z. P. Zhuang, M. P. Kung, C. Hou, K. Ploessl, and H. F. Kung, "Biphenyls labeled with technetium 99m for imaging $\beta$-amyloid plaques in the brain," *Nuclear Medicine and Biology*, vol. 32, no. 2, pp. 171–184, 2005.

[55] K. S. Lin, M. L. Debnath, C. A. Mathis, and W. E. Klunk, "Synthesis and $\beta$-amyloid binding properties of rhenium 2-phenylbenzothiazoles," *Bioorganic and Medicinal Chemistry Letters*, vol. 19, no. 8, pp. 2258–2262, 2009.

[56] S. Oya, K. Plössl, M. P. Kung, D. A. Stevenson, and H. F. Kung, "Small and neutral TC(V)O BAT, bisaminoethanethiol (NS) complexes for developing new brain imaging agents," *Nuclear Medicine and Biology*, vol. 25, no. 2, pp. 135–140, 1998.

[57] M. Ono, R. Ikeoka, H. Watanabe et al., "Synthesis and evaluation of novel chalcone derivatives with $^{99m}$Tc/Re complexes as potential probes for detection of $\beta$-amyloid plaques," *ACS Chemical Neuroscience*, vol. 1, no. 9, pp. 598–607, 2010.

Bioorganic & Medicinal Chemistry 19 (2011) 3216–3220

Contents lists available at ScienceDirect

Bioorganic & Medicinal Chemistry

journal homepage: www.elsevier.com/locate/bmc

# Concise site-specific synthesis of DTPA–peptide conjugates: Application to imaging probes for the chemokine receptor CXCR4

Ryo Masuda, Shinya Oishi *, Hiroaki Ohno, Hiroyuki Kimura, Hideo Saji, Nobutaka Fujii *

*Graduate School of Pharmaceutical Sciences, Kyoto University, Sakyo-ku, Kyoto 606-8501, Japan*

ARTICLE INFO

*Article history:*
Received 17 February 2011
Revised 25 March 2011
Accepted 26 March 2011
Available online 2 April 2011

*Keywords:*
CXCR4
DTPA
Molecular imaging

ABSTRACT

Diethylenetriaminepentaacetic acid (DTPA) is a useful chelating agent for radionuclides such as $^{68}$Ga, $^{99m}$Tc and $^{111}$In, which are applicable to nuclear medicine imaging. In this study, we established a facile synthetic protocol for the production of mono-DTPA-conjugated peptide probes. A novel monoreactive DTPA precursor reagent was synthesized in two steps using the chemistry of the *o*-nitrobenzenesulfonyl (Ns) protecting group, and under mild conditions this DTPA precursor was incorporated onto an $N^{\varepsilon}$-bromoacetylated Lys of a protected peptide resin. The site-specific DTPA conjugation was facilitated by using a highly acid-labile 4-methyltrityl (Mtt) protecting group for the target site of the bioactive peptide during the solid-phase synthesis. A combination of both techniques yielded peptides with disulfide bonds, such as octreotide and polyphemusin II-derived CXCR4 antagonists. DTPA–peptide conjugates were purified in a single step following cleavage from the resin and disulfide bond formation. This site-specific on-resin construction strategy was used for the design and synthesis of a novel In-DTPA-labeled CXCR4 antagonist, which exhibited highly potent inhibitory activity against SDF-1–CXCR4 binding.



## 1. Introduction

Recent progress in molecular imaging methodologies such as positron emission tomography (PET), single-photon emission computed tomography (SPECT) and optical imaging technologies has significantly improved the early detection and diagnosis of malignant tumors. To visualize the specific molecular events involved in the physiological and/or pathological processes, a number of peptide-based imaging probes have been developed for overexpressed receptors of peptide hormones and extracellular matrix proteins.[1] These probes are usually designed by a combination of three components: a target-specific vector peptide, an imaging part such as a radionuclide or fluorophore, and a linker to covalently or noncovalently conjugate the peptide with the imaging moiety. The addition of a functional moiety onto small-sized bioactive peptides may be highly susceptible to interaction with receptors or counterpart molecules. Consequently, there have been many reagents of choice for appropriate protein/peptide modifications. In addition, to determine the best labeling position from structure-function relationship studies, versatile synthetic approaches toward various types of labeled peptide are desired.

Polyamino polycarboxylate ligands efficiently coordinate metal radioisotopes to aid the radiolabeling of bioactive peptides. Among the chelating ligands, 1,4,7,10-tetraazacyclododecane-1,4,7,10-tetraacetic acid (DOTA) **1a** has been most widely utilized, since a variety of metal radioisotopes for both diagnostic and therapeutic purposes form complexes with high affinity and kinetic stability (Fig. 1).[2] DOTA-modification of bioactive peptides is facilitated by commercially available reagents such as DOTA-NHS **1b** and DOTA-maleimide **1c** to provide the expected peptides in a single step.[3,4] Alternatively, tris(*tert*-butyl)-DOTA **2a** with a free carboxyl group is employed for the modification of an amino group of protected peptides bound to solid-supports.[5] Lysine or phenylalanine derivatives **2b,c** possessing a *tert*-butyl-protected DOTA moiety are also useful components for the peptide sequence assembly.[6] *tert*-Butyl protecting groups in these reagents are easily removed during the final side-chain deprotection process of peptide synthesis.

In contrast to these DOTA derivatives, there has been limited work exploring the application of the diethylenetriaminepentaacetic acid (DTPA) chelating group **3a**, although DTPA represents a promising alternative, especially for $^{68}$Ga, $^{99m}$Tc and $^{111}$In (Fig. 1). The recent success of DTPA-based probes is exemplified by a glucagon-like peptide-1 (GLP-1) receptor ligand, [Lys$^{40}$(Ahx-DTPA-$^{111}$In)$NH_2$]-exendin-4, for insulinoma diagnosis.[7] The DTPA group also works as a more favorable functional group than DOTA to facilitate the biological or biodistribution properties of several probes.[8] For the preparation of DTPA-conjugated imaging probes, several conjugation reagents have been developed. The most familiar cyclic diethylenetriaminepentaacetic dianhydride **4**

* Corresponding authors. Tel.: +81 75 753 4551; fax: +81 75 753 4570.
*E-mail addresses:* soishi@pharm.kyoto-u.ac.jp (S. Oishi), nfujii@pharm.kyoto-u.ac.jp (N. Fujii).

0968-0896/$ - see front matter © 2011 Elsevier Ltd. All rights reserved.
doi:10.1016/j.bmc.2011.03.059

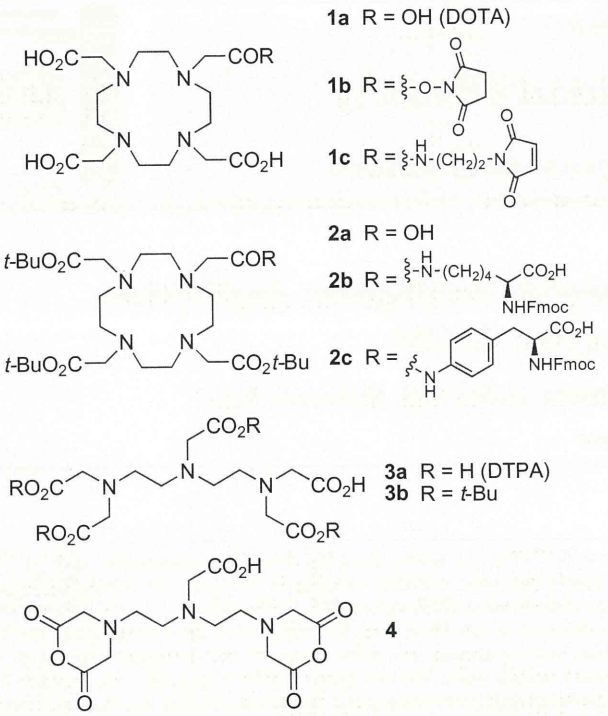


**Figure 1.** Structures of radionuclide chelating agents and the precursors.

is a bifunctional chelating agent, which can conjugate with peptide hormones and antibodies.[9] Using this reagent, concomitant formations of a bis-conjugated product[10] and intra- and intermolecular cross-linked products[11] were unavoidable. Monoreactive DTPA derivatives have also been developed for the preparation of DTPA–peptide conjugates without the unfavorable by-product formations.[12,13] For example, we reported the synthesis and application of 3,6,9,9-tetrakis[(*tert*-butoxycarbonyl)methyl]-3,6,9-triazanonanoic acid **3b** (mDTPA),[14] in which the four carboxylates were protected with *tert*-butyl ester. However, a longer process from the commercially available reagents is required for the synthesis of these DTPA-conjugation reagents (Scheme 1A).

Accordingly, to establish a facile and efficient synthetic method for DTPA–peptide conjugates, we have investigated the site-specific and on-resin construction of a DTPA moiety. Herein, we describe the short-step synthesis of a DTPA precursor using the *o*-nitrobenzenesulfonyl (Ns) protecting group and the solid-phase synthesis of DTPA–peptide conjugates. The design and synthesis of DTPA–peptide conjugates that potentially target the somatostatin receptor and chemokine receptor CXCR4 are also presented.[15]

## 2. Results and discussion

### 2.1. Synthesis of a DTPA-conjugation reagent and the application to octreotide derivatives

The synthetic scheme for the production of mDTPA reagent **10**, as described in our previous study, is presented in Scheme 1A. We hypothesized that two remedies could significantly improve the overall synthetic process of DTPA–peptide conjugates. First, the use of an Ns group in place of the trifluoroacetyl group was expected to serve as a temporary protecting group and an auxiliary group for global modification with four *tert*-butoxycarbonylmethyl groups. This potentially improves the stepwise synthesis of the intermediate **7** in the solution-phase. In addition, a secondary amine **8** as a nucleophilic precursor for the bromoacetyl group on peptide resin **11** can directly produce the overall DTPA framework of **12** on the solid support without the additional three-step modification process of **8** in solution (Scheme 1B).[16]

Synthesis of DTPA precursor **8** began with mono-Ns protection of the commercially available diethylenetriamine **5** (Scheme 2). The Ns-protected intermediate was successively treated with excess equivalent of *t*-butyl bromoacetate in a one-pot process. Although the solvent EtOH has been reported to be effective in predominantly giving the mono-Ns product,[17] concomitant production of bis-Ns product **14b** was not suppressed as in DMF. The treatment of excess diethylenetriamine **5** with NsCl in EtOH provided mono-Ns product **14a** in 65% yield (calculated based on NsCl), which can be readily purified by chromatography. Compound **14a** was then subjected to deprotection with mercaptoacetic acid and LiOH to provide the expected precursor **8** in 77% yield.

Using the resulting reagent **8**, DTPA-conjugation of [D-Phe$^1$]octreotide was investigated as a model study (Scheme 3), which is employed as a radionuclide imaging probe for the somatostatin receptor.[14,18,19] After peptide-chain elongation by Fmoc-based solid-phase peptide synthesis, the N-terminus of **16** was modified with bromoacetic acid and 1,3-diisopropylcarbodiimide (DIC). Subsequently, the bromide **17** was treated with the reagent **8** in the presence of $(i\text{-Pr})_2$NEt to provide the fully protected peptide resin **18a**. Cleavage from the resin **18a** and disulfide formation under air-oxidation conditions provided [DTPA-D-Phe$^1$]octreotide **19a** with high purity. The bromoacetylated peptide **17** was also modified with commercially available DOTA precursor reagent **20**, using the identical procedure to provide [DOTA-D-Phe$^1$]octreotide **19b**.[20] These suggest that this on-resin modification procedure is widely applicable to any chelating reagents with nucleophilic functional groups such as DTPA and DOTA precursors.

### 2.2. Site-specific DTPA-conjugation of bioactive peptides: synthesis of CXCR4 receptor probes

It has been reported that a high level of CXCR4 expression in tumors is associated with malignant and metastatic properties.[21] Intrinsic SDF-1 release from the potential distal metastatic sites mediates organ-specific metastasis of CXCR4-expressing cells from the primary lesions. Since CXCR4-expressing cancer stem cells are related to the metastatic spread in orthotopic primary tumors,[22] it is of considerable importance to develop potent CXCR4-imaging probes to detect potential cancer stem cells within malignant tumors, as exemplified by the diagnosis of bladder cancer by a fluorescent CXCR4 probe.[23,24]

Previously, we reported a DTPA-conjugated CXCR4 antagonist, DTPA-Ac-TZ14011 **26a**,[25] which was designed from a horseshoe crab-derived anti-HIV peptide T140. This peptide has β-sheet-like structures maintained by a disulfide bond, around which the pharmacophore residues for bioactivity are located.[26] For the site-specific conjugation at D-Lys$^8$ in the type II' β-turn region of T140 with a single DTPA group in the solution-phase, a secondary lysine (Lys$^7$) was substituted with arginine, which cannot be acylated by standard reagents.[25] Although a DTPA group was successfully ligated with maintenance of highly potent CXCR4 antagonistic activity in this case,[25] the accompanying substitutions needed for specific modification of other peptides may possibly lead to a decrease in the bioactivity. Therefore, we planned the facile site-specific DTPA conjugation on a solid-support for production of CXCR4 imaging probes without substitution of the secondary Lys$^7$ residue. To distinguish D-Lys$^8$ to be labeled in peptides **26**, the highly acid-labile 4-methyltrityl (Mtt) group was exploited for temporary protection of the ε-amino group during solid-phase peptide synthesis.[27] For the other Lys residues such as Lys$^7$ of

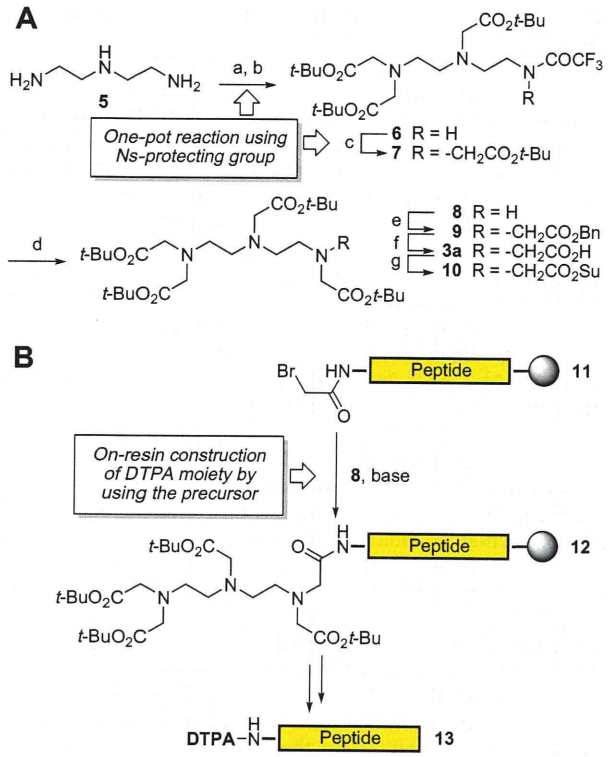


**Scheme 1.** (A) Synthetic scheme for the DTPA-conjugation reagent **10** prepared in our previous study; (B) synthetic plan for the DTPA-conjugated peptides in this study. Reagents: (a) $CF_3CO_2Et$; (b) $BrCH_2CO_2t$-Bu, $(i\text{-}Pr)_2NEt$; (c) $BrCH_2CO_2t$-Bu, NaH; (d) $NH_2NH_2$, *t*-BuOH; (e) $BrCH_2CO_2Bn$, $(i\text{-}Pr)_2NEt$; (f) $H_2$, Pd/C; (g) DCC, HOSu.

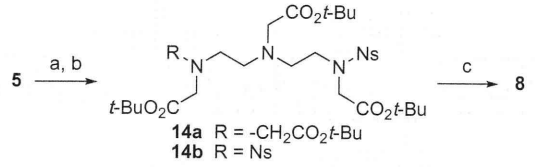


**Scheme 2.** Synthesis of DTPA precursor **8** via a global N-alkylation process using a Ns-protecting group. Reagents: (a) NsCl; (b) $BrCH_2CO_2t$-Bu, $K_2CO_3$; (c) $HSCH_2CO_2H$, LiOH.

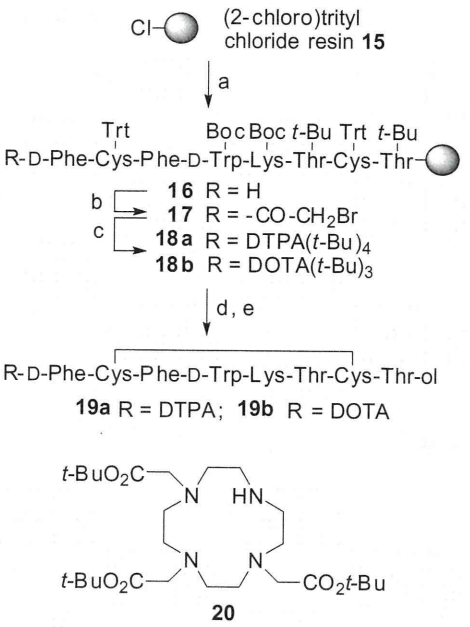


**Scheme 3.** Synthesis of DTPA- and DOTA-conjugated D-Phe-octreotides. Reagents: (a) Fmoc-based peptide synthesis; (b) $BrCH_2CO_2H$, DIC; (c) **8** for **18a**, or **20** for **18b**, $(i\text{-}Pr)_2NEt$ (d) TFA/$H_2O$/1,2-ethanedithiol (EDT) (95:2.5:2.5) for **19a**, 1 M TMSBr, thioanisole/TFA, 1,2-ethanedithiol, *m*-cresol for **19b**; (e) $NH_4OH$ (air oxidation).

**26b,c**, a Boc group was employed. This group can be cleaved by the standard TFA-based treatment in Fmoc chemistry (Scheme 4). After the construction of the protected peptide resin, the orthogonal Mtt group at the labeling position was cleaved off using 1,1,1,3,3,3-hexafluoropropan-2-ol (HFIP). The resulting ε-amino group was successively modified with bromoacetic acid followed by the reagent **8** to provide the fully protected DTPA–peptide resin **25**. Final deprotection, air-oxidation and HPLC purification afforded the expected DTPA-conjugated CXCR4 antagonists **26a,b**. This concise protocol facilitates the selection of chelating structure and position(s) on the peptide chain, and aids structure–activity relationship studies aimed at exploring the more potent peptide probes. For example, a 4-fluorobenzoyl modification at the N-terminus, which should increase CXCR4 antagonism,[28] was easily appended to the peptide using this protocol to give the modified peptide **26c**. The subsequent treatment with nonradioactive $InCl_3$ in acidic conditions provided the In-DTPA-labeled CXCR4 antagonists **27a–c**.

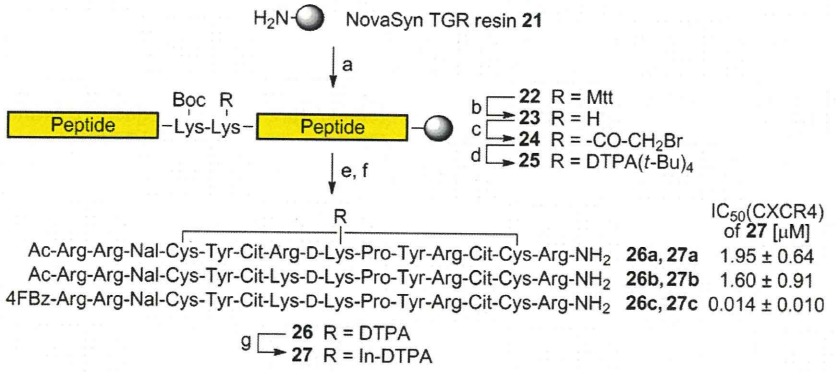


**Scheme 4.** Site-specific In-DTPA labeling of CXCR4 antagonists and biological activity. Reagents: (a) Fmoc-based peptide synthesis; (b) $CH_2Cl_2$/1,1,1,3,3,3-hexafluoro-2-propanol (HFIP)/2,2,2-trifluoroethanol (TFE)/triethylsilane (TES) (65:20:10:5); (c) $BrCH_2CO_2H$, DIC; (d) **8**, $(i\text{-}Pr)_2NEt$; (e) TFA/$H_2O$/EDT (95:2.5:2.5); (f) $NH_4OH$ (air oxidation); (g) $InCl_3$. *Abbreviations:* Mtt: 4-methyltrityl; Cit: L-citrulline, Nal: L-3-(2-naphthyl)alanine, 4FBz: 4-fluorobenzoyl.

### 2.3. Bioactivity of In-DTPA-labeled CXCR4 antagonists

The biological activity of the In-DTPA-labeled peptides **27a–c** was evaluated as the inhibitory potency of [$^{125}$I]-SDF-1-binding to CXCR4 membrane extracts (Scheme 4). Peptides **27a,b**, with an N-terminal acetyl group, exhibited similar potency towards CXCR4 [$IC_{50}$(**27a**) = 1.95 ± 0.64 μM, $IC_{50}$(**27b**) = 1.60 ± 0.91 μM], indicating that the Lys and Arg for the *i*-position of β-turn were both tolerant to the bioactivity. In contrast, peptide **27c** exerted much more potent inhibitory activity for the SDF-1 binding to CXCR4 [$IC_{50}$(**27c**) = 0.014 ± 0.010 μM]. These results of In-DTPA-labeled peptides **27a–c** coincided with our previous report on the unlabeled peptides.[28] The novel potent In-DTPA-labeled CXCR4 antagonist **27c** could be a promising imaging probe for CXCR4-expressing malignant cancer cells.[11]

## 3. Conclusions

In this study, we have established a novel synthetic method for the production of DTPA–peptide conjugates. The process includes facile solid-phase synthesis of a DTPA framework using a novel precursor substrate and site-specific conjugation using a highly acid-labile protecting group. Using a temporary Ns protecting group, the DTPA precursor **8** was obtained through two purification steps from commercially available diethylenetriamine. In addition, the on-resin incorporation of a bromoacetyl group into the specific free amino group followed by the addition of the nucleophilic DTPA precursors provided the expected DTPA–peptide conjugates with high purity. Taking advantage of secondary amine precursors of choice, these processes represent versatile methods to prepare a series of peptide conjugates, including DTPA and DOTA, for optimization of imaging probes. This conjugation method was applied to the preparation of DTPA-conjugates of octreotide and CXCR4 antagonist, which have been reported to effectively detect cancer cells. The peptide **27c** with highly potent inhibitory activity of SDF-1 binding to CXCR4 was obtained without any amino acid substitution to avoid multiple modifications on the amino groups. This peptide represents a promising lead compound as an imaging probe towards CXCR4-positive metastatic tumors.

## 4. Experimental

### 4.1. Synthesis

#### 4.1.1. Bis(*tert*-butyl) 3,6-bis[(*tert*-butoxycarbonyl)methyl]-9-(*o*-nitrobenzenesulfonyl)-3,6,9-triazaundecanedioate (14a)

To diethylenetriamine **5** (0.540 mL, 5.00 mmol) in dehydrated EtOH (5 mL), *o*-NsCl (0.367 g, 1.67 mmol) was slowly added below 0 °C. After stirring for 2 h, EtOH was removed in vacuo. To dehydrated DMF (8 mL), $K_2CO_3$ (4.49 g, 32.5 mmol) and $BrCH_2CO_2t$-Bu (4.06 mL, 27.5 mmol) were added at 0 °C. The mixture was stirred overnight at room temperature, and filtered. The filtrate was concentrated under reduced pressure to give an oily residue, and the residue was dissolved in EtOAc (100 mL). The whole mixture was washed with saturated $NaHCO_3$, and was dried over $MgSO_4$. Concentration under reduced pressure followed by flash chromatography over silica gel with *n*-hexane–EtOAc gave compound **14a** as a yellow oil (0.81 g, 65%); $^1$H NMR ($CDCl_3$, 500 MHz) δ 8.08–8.11 (1H, m), 7.64–7.69 (2H, m), 7.56–7.60 (1H, m), 4.24 (2H, s), 3.49 (2H, t, *J* = 6.9 Hz), 3.42 (4H, s), 3.30 (2H, s), 2.88 (2H, t, *J* = 6.6 Hz), 2.78 (2H, t, *J* = 6.9 Hz), 2.77 (2H, t, *J* = 6.9 Hz), 1.45 (27H, s), 1.36 (9H, s); $^{13}$C NMR ($CDCl_3$, 500 MHz) δ 170.6 (3C), 168.0, 133.7, 133.2, 131.6 (2C), 130.9, 123.9, 82.0, 81.0, 80.9 (2C), 56.1 (3C), 53.3, 52.8, 52.4, 49.4, 46.7, 28.1 (9C), 27.9 (3C); HRMS (FAB) *m*/*z* calcd for $C_{34}H_{58}N_4O_{12}S$ ([M+H]$^+$): 746.3772, found 746.3779.

#### 4.1.2. Bis(*tert*-butyl) 3,6-bis[(*tert*-butoxycarbonyl)methyl]-3,6,9-triazaundecanedioate (8)

To a solution of compound **14a** (0.216 g, 0.29 mmol) in DMF (0.726 mL), LiOH (0.128 g, 2.90 mmol) and mercaptoacetic acid (0.101 mL, 1.45 mmol) were added below 0 °C. After stirring for 2 h at room temperature, the mixture was concentrated under reduced pressure, and the residue was dissolved in $CHCl_3$. The whole reaction mixture was washed with saturated $NaHCO_3$, and was dried over $Na_2SO_4$. Concentration under reduced pressure followed by flash chromatography over silica gel with $CHCl_3$–MeOH gave compound **8** as a yellow oil (0.124 g, 77%); $^1$H NMR ($CDCl_3$, 500 MHz) δ 3.39 (4H, s), 3.28 (4H, s), 2.72–2.82 (6H, m), 2.63 (2H, t, *J* = 5.4 Hz), 1.39 (9H, s), 1.38 (27H, s); $^{13}$C NMR ($CDCl_3$, 500 MHz) δ 170.9, 170.7 (3C), 80.8 (4C), 55.9 (2C), 55.8 (2C), 52.4, 52.3, 51.3, 47.0, 28.2 (3C), 28.1 (9C); HRMS (FAB) *m*/*z* calcd for $C_{28}H_{54}N_3O_8$ ([M+H]$^+$): 560.3911, found 560.3910.

#### 4.1.3. Standard procedure for solid-phase peptide synthesis

Protected peptide-resins were manually constructed by Fmoc-based solid-phase peptide synthesis. *t*-Bu ester for Asp and Glu; 2,2,4,6,7-pentamethyldihydrobenzofurane-5-sulfonyl (Pbf) for Arg; *t*-Bu for Thr and Tyr; Boc for Lys and Trp; Trt for Cys were employed for side-chain protection. Fmoc-amino acids were coupled using three equivalents of reagents [Fmoc-amino acid, 1,3-diisopropylcarbodiimide (DIC), and HOBt·$H_2O$] to the free amino group in DMF for 1.5 h. Fmoc deprotection was performed by 20% (v/v) piperidine in DMF (2 × 1 min, 1 × 30 min). The protected peptide resin was treated with a cocktail of deprotection reagents. After removal of the resin by filtration, the filtrate was poured into ice-cold dry $Et_2O$. The resulting powder was collected by centrifugation and washed with ice-cold dry $Et_2O$. The crude peptide was dissolved in $H_2O$, and the pH was adjusted to 8.0 with $NH_4OH$ for disulfide bond formation. After air-oxidation for 1 d, the crude product was purified by preparative HPLC on a Cosmosil 5C18-ARII preparative column (Nacalai Tesque, Kyoto, Japan; 20 × 250 mm, flow rate 10 mL/min) to afford the expected peptides. All peptides were characterized by MALDI-TOF-MS (AXIMA-CFR plus, Shimadzu, Kyoto, Japan) and the purity was calculated as >95% by HPLC on a Cosmosil 5C18-ARII analytical column (Nacalai Tesque, 4.6 × 250 mm, flow rate 1 mL/min) at 220 nm absorbance.

#### 4.1.4. Preparation of DTPA- and DOTA-conjugated octreotides (19a,b)

According to the procedure reported previously,[18] (2-chloro)trityl chloride resin **15** (214 mg, 1.4 mmol/g), Fmoc-Thr(*t*-Bu)-ol (345 mg, 0.9 mmol), and pyridine (0.145 mL, 1.8 mmol) were agitated for 21 h in dry $CH_2Cl_2$–DMF (1:1, 3.94 mL). The loading was determined by measuring the 290 nm UV absorption of the piperidine-treated sample (0.455 mmol/g). After the construction of the peptide chain (0.017 mmol scale) using a standard procedure, bromoacetic acid (23.6 mg, 0.17 mmol) with DIC (0.026 mL, 0.17 mmol) in $CH_2Cl_2$ was reacted with resin **16** for 2 h at room temperature. The subsequent treatment of **17** with amines **8** (29.0 mg, 0.51 mmol) and **20** (26.3 mg, 0.51 mmol) with ($i$-Pr)$_2$NEt (0.009 mL, 0.51 mmol) in DMF for 12 h at room temperature provided **18a** and **18b**, respectively. Cleavage and deprotection of **18a** (72.5 mg) and **18b** (73.8 mg) was achieved using a TFA/1,2-ethandithiol (EDT)/$H_2O$ (5 mL; 95:2.5:2.5) cocktail for 2 h at room temperature and by treatment with 1 M TMSBr-thioanisole/TFA in the presence of EDT/*m*-cresol (3.3 mL) for 2 h at 0 °C, respectively. After disulfide formation under air-oxidation conditions, the crude peptides were purified using the standard procedure, to afford the desired peptides **19a** (8.2 mg, 23%) and **19b** (9.5 mg, 26%) as white powders. Compound **19a**: MS (MALDI-TOF) *m*/*z* calcd for $C_{63}H_{89}N_{13}O_{19}S_2$ ([M+H]$^+$): 1395.6, found 1395.3. Compound **19b**:

MS (MALDI-TOF) $m/z$ calcd for $C_{65}H_{93}N_{14}O_{17}S_2$ ($[M+H]^+$): 1405.6, found 1405.8.

#### 4.1.5. Preparation of DTPA-conjugated CXCR4 antagonists (26a–c)

Protected peptide resins were manually constructed according to the standard procedure using NovaSyn TGR-resin **21** (96.2 mg, 0.025 mmol). 4-Methyltrityl (Mtt) group was employed for the protection of the D-Lys ε-amino group. The N-terminal amino group was acylated by treatment with $Ac_2O$ (0.012 mL, 0.125 mmol)/pyridine (0.020 mL, 0.250 mmol) for 1 h at room temperature for peptides **26a,b**, and with 4-fluorobenzoic acid (17.5 mg, 0.125 mmol)/DIC (0.019 mL, 0.125 mmol)/HOBt·$H_2O$ (19.2 mg, 0.125 mmol) for 1.5 h at room temperature for peptide **26c**. Subsequently, the resin **22** was treated with $CH_2Cl_2$/1,1,1,3,3,3-hexafluoropropan-2-ol (HFIP)/trifluoroethanol (TFE)/triethylsilane (TES) [65:20:10:5; 5 mL] for 2 h at room temperature. The DTPA group was incorporated using the identical procedure employed for the synthesis of the octreotide derivative **19a**. Treatment of the resins (**25a**: 178 mg, **25b**: 165 mg, **25c**: 162 mg) with a TFA/1,2-ethandithiol(EDT)/$H_2O$ (95:2.5:2.5; 5 mL) cocktail for 2 h at room temperature followed by air oxidation and purification provided the peptides Compound **26a** (14.6 mg, 15.4%), **26b** (6.67 mg, 8.7%) and **26c** (7.4 mg, 9.5%) as white powders. Compound **26a:** MS (MALDI-TOF) $m/z$ calcd for $C_{106}H_{165}N_{38}O_{28}S_2$ ($[M+H]^+$): 2482.2, found 2482.5. Compound **26b**: MS (MALDI-TOF) $m/z$ calcd for $C_{106}H_{165}N_{36}O_{28}S_2$ ($[M+H]^+$): 2454.2, found 2453.9. Compound **26c**: MS (MALDI-TOF) $m/z$ calcd for $C_{111}H_{166}FN_{36}O_{28}S_2$ ($[M+H]^+$): 2534.2, found 2533.8.

#### 4.1.6. Indium chelating for CXCR4 antagonist probes (27a–c)

To a solution of peptides **26a–c** (8 mM in 0.1 N AcOH, **26a**: 45.9 μL, 0.37 μmol; **26b**: 48.4 μL, 0.39 μmol; **26c**: 48.8 μL, 0.39 μmol), $InCl_3$ (1 M in 0.02 N HCl, 50 μL) was added and the solution stirred for a further 30 min at room temperature. HPLC purification using a standard procedure provided the desired peptides **27a** (0.43 mg, 36.7%), **27b** (0.42 mg, 34.3%) and **27c** (0.38 mg, 30.3%) as white powders. Compound **27a**: MS (MALDI-TOF) $m/z$ calcd for $C_{106}H_{165}InN_{38}O_{28}S_2$ ($[M+H]^+$): 2597.1, found 2596.9. Compound **27b**: MS (MALDI-TOF) $m/z$ calcd for $C_{106}H_{165}InN_{36}O_{28}S_2$ ($[M+H]^+$): 2569.1, found 2569.1. Compound **27c**: MS (MALDI-TOF) $m/z$ calcd for $C_{111}H_{166}FInN_{36}O_{28}S_2$ ($[M+H]^+$): 2649.1, found 2649.0.

### 4.2. Evaluation of [$^{125}$I]-SDF-1 binding and displacement

For ligand binding, the CXCR4 membrane was incubated with 0.5 nM of [$^{125}$I]-SDF-1 and increasing concentrations of compounds **27a–c** in binding buffer [50 mM HEPES (pH 7.4), 5 mM $MgCl_2$, 1 mM $CaCl_2$ and 0.1% BSA in $H_2O$] for 1 h at room temperature. The reaction mixtures were filtered through GF/B filters (Perkin-Elmer, Wellesley, MA) pretreated with 0.1% polyethyleneimine. The filter plate was washed with wash buffer [50 mM HEPES (pH 7.4), 500 mM NaCl and 0.1% BSA in $H_2O$] and the bound radioactivity was measured by TopCount (Packard, Meriden, CT). Inhibitory activity of test compounds was determined based on the inhibition of [$^{125}$I]-SDF-1 binding to the CXCR4 receptor ($IC_{50}$).


## Acknowledgments

This work is supported by Grants-in-Aid for Scientific Research and Molecular Imaging Research Program from the Ministry of Education, Culture, Sports, Science, and Technology of Japan. R.M. is grateful for Research Fellowships from the JSPS for Young Scientists.


## Supplementary data

Supplementary data associated with this article can be found, in the online version, at doi:10.1016/j.bmc.2011.03.059.

## References and notes


1. Lee, S.; Xie, J.; Chen, X. *Chem. Rev.* **2010**, *110*, 3087.
2. De León-Rodríguez, L. M.; Kovacs, Z. *Bioconjugate Chem.* **2008**, *19*, 391.
3. Mier, W.; Hoffend, J.; Krmer, S.; Schuhmacher, J.; Hull, W. E.; Eisenhut, M.; Haberkorn, U. *Bioconjugate Chem.* **2005**, *16*, 237.
4. Lewis, M. R.; Shively, J. E. *Bioconjugate Chem.* **1998**, *9*, 72.
5. Heppeler, A.; Froidevaux, S.; Mäcke, H. R.; Jermann, E.; Powell, P.; Henning, M. *Chem. Eur. J.* **1999**, *5*, 1974.
6. De León-Rodriguez, L. M.; Kovacs, Z.; Dieckmann, G. R.; Sherry, A. D. *Chem. Eur. J.* **2004**, *10*, 1149.
7. Wild, D.; Wicki, A.; Mansi, R.; Béhé, M.; Keil, B.; Bernhardt, P.; Christofori, G.; Ell, P. J.; Mäcke, H. R. *J. Nucl. Med.* **2010**, *51*, 1059, and the references therein.
8. De Jong, M.; Breeman, W. A.; Bakker, W. H.; Kooij, P. P.; Bernard, B. F.; Hofland, L. J.; Visser, T. J.; Srinivasan, A.; Schmidt, M. A.; Erion, J. L.; Bugaj, J. E.; Mäcke, H. R.; Krenning, E. P. *Cancer Res.* **1998**, *58*, 437.
9. Hnatowich, D. J.; Layne, W. W.; Childs, R. L. *Int. J. Appl. Radiat. Isot.* **1982**, *33*, 327.
10. Wang, S.; Luo, J.; Lantrip, D. A.; Waters, D. J.; Mathias, C. J.; Green, M. A.; Fuchs, P. L.; Low, P. S. *Bioconjugate Chem.* **1997**, *8*, 673.
11. Reilly, R.; Lee, N.; Houle, S.; Law, J.; Marks, A. *Appl. Radiat. Isot.* **1992**, *43*, 961.
12. Hnatowich, D. J.; Layne, W. W.; Childs, R. L.; Lanteigne, D.; Davis, M. A.; Griffin, T. W.; Doherty, P. W. *Science* **1983**, *220*, 613.
13. Van Hagen, P. M.; Breeman, W. A. P.; Bernard, H. F.; Schaar, M.; Mooij, C. M.; Srinivasan, A.; Schmidt, M. A.; Krenning, E. P.; De Jong, M. *Int. J. Cancer* **2000**, *90*, 186.
14. Arano, Y.; Uezono, T.; Akizawa, H.; Ono, M.; Wakisaka, K.; Nakayama, M.; Sakahara, H.; Konishi, J.; Yokoyama, A. *J. Med. Chem.* **1996**, *39*, 3451.
15. A portion of this study was reported in a preliminary communication: Masuda, R.; Ohno, H.; Oishi, S.; Fujii, N. In *Pepide Science*, Okamoto, Ed.; 2009, p 159.
16. Peterson, J. J.; Pak, R. H.; Meares, C. F. *Bioconjugate Chem.* **1999**, *10*, 316.
17. Hidai, Y.; Kan, T.; Fukuyama, T. *Chem. Pharm. Bull.* **2000**, *48*, 1570.
18. Arano, Y.; Akizawa, H.; Uezono, T.; Akaji, K.; Ono, M.; Funakoshi, S.; Koizumi, M.; Yokoyama, A.; Kiso, Y.; Saji, H. *Bioconjugate Chem.* **1997**, *8*, 442.
19. Lewis, J. S.; Anderson, C. J. *Methods Mol. Biol.* **2007**, *386*, 227.
20. Albert, R.; Smith-Jones, P.; Stolz, B.; Simeon, C.; Knecht, H.; Bruns, C.; Pless, J. *Bioorg. Med. Chem. Lett.* **1998**, *8*, 1207.
21. Müller, A.; Homey, B.; Soto, H.; Ge, N.; Catron, D.; Buchanan, M. E.; McClanahan, T.; Murphy, E.; Yuan, W.; Wagner, S. N.; Barrera, J. L.; Mohar, A.; Verástegui, E.; Zlotnik, A. *Nature* **2001**, *410*, 50.
22. Hermann, P. C.; Huber, S. L.; Heeschen, C. *Cell Cycle* **2008**, *7*, 188.
23. Oishi, S.; Masuda, R.; Evans, B.; Ueda, S.; Goto, Y.; Ohno, H.; Hirasawa, A.; Tsujimoto, G.; Wang, Z.; Peiper, S. C.; Naito, T.; Kodama, E.; Matsuoka, M.; Fujii, N. *ChemBioChem* **2008**, *9*, 1154.
24. Nishizawa, K.; Nishiyama, H.; Oishi, S.; Tanahara, N.; Kotani, H.; Mikami, Y.; Toda, Y.; Evans, B. J.; Peiper, S. C.; Saito, R.; Watanabe, J.; Fujii, N.; Ogawa, O. *Int. J. Cancer* **2010**, *127*, 1180.
25. Hanaoka, H.; Mukai, T.; Tamamura, H.; Mori, T.; Ishino, S.; Ogawa, K.; Iida, Y.; Doi, R.; Fujii, N.; Saji, H. *Nucl. Med. Biol.* **2006**, *33*, 489.
26. Tamamura, H.; Omagari, A.; Oishi, S.; Kanamoto, T.; Yamamoto, N.; Peiper, S. C.; Nakashima, H.; Otaka, A.; Fujii, N. *Bioorg. Med. Chem. Lett.* **2000**, *10*, 2633.
27. Stephenson, K. A.; Banerjee, S. R.; McFarlane, N.; Boreham, D. R.; Maresca, K. P.; Babich, J. W.; Zubieta, J.; Valliant, J. F. *Can. J. Chem.* **2005**, *83*, 2060.
28. Tamamura, H.; Hiramatsu, K.; Mizumoto, M.; Ueda, S.; Kusano, S.; Terakubo, S.; Akamatsu, M.; Yamamoto, N.; Trent, J. O.; Wang, Z.; Peiper, S. C.; Nakashima, H.; Otaka, A.; Fujii, N. *Org. Biomol. Chem.* **2003**, *1*, 3663.

Available online at www.sciencedirect.com
ScienceDirect
Nuclear Medicine and Biology 38 (2011) 313–320
NUCLEAR MEDICINE — AND — BIOLOGY
www.elsevier.com/locate/nucmedbio

# Radioiodinated benzimidazole derivatives as single photon emission computed tomography probes for imaging of β-amyloid plaques in Alzheimer's disease

Mengchao Cui[a,b], Masahiro Ono[a,*], Hiroyuki Kimura[a], Hidekazu Kawashima[a], Bo Li Liu[b], Hideo Saji[a,*]

[a]*Graduate School of Pharmaceutical Sciences, Kyoto University, Kyoto 606-8501, Japan*
[b]*Key Laboratory of Radiopharmaceuticals, Ministry of Education, College of Chemistry, Beijing Normal University, Beijing 100875, P.R. China*

Received 20 July 2010; received in revised form 16 September 2010; accepted 28 September 2010

**Abstract**

Five iodinated 2-phenyl-1H-benzo[*d*]imidazole derivatives were synthesized and evaluated as potential probes for β-amyloid (Aβ) plaques. One of the compounds, 4-(6-iodo-1H-benzo[*d*]imidazol-2-yl)-*N*,*N*-dimethylaniline (**12**), showed excellent affinity for $A\beta_{1\text{-}42}$ aggregates ($K_i$=9.8 nM). Autoradiography with sections of postmortem Alzheimer's disease (AD) brain revealed that a radioiodinated probe [$^{125}$I]**12**, labeled Aβ plaques selectively with low nonspecific binding. Biodistribution experiments with normal mice injected intravenously with [$^{125}$I]**12** showed high uptake [4.14 percent injected dose per gram (% ID/g) at 2 min] into and rapid clearance (0.15% ID/g at 60 min) from the brain, which may bring about a good signal-to-noise ratio and therefore achieve highly sensitive detection of Aβ plaques. In addition, [$^{125}$I]**12** labeled amyloid plaques in vivo in an AD transgenic model. The preliminary results strongly suggest that [$^{125}$I]**12** bears characteristics suitable for detecting amyloid plaques in vivo. When labeled with $^{123}$I, it may be a useful SPECT imaging agent for Aβ plaques in the brain of living AD patients.


*Keywords:* Alzheimer's disease; β-Amyloid; Single photon emission computed tomography (SPECT); Imaging agent

## 1. Introduction

Alzheimer's disease (AD) is an age-related, irreversible form of dementia characterized by memory loss, a progressive decline in intellectual ability, language impairment and personality and behavioral changes that eventually interfere with daily life [1]. The accumulation of β-amyloid (Aβ) aggregates (major protein aggregates of senile plaques) in the brain is considered one of the hallmarks of AD [2,3]. Today, the clinical diagnosis of AD is primarily based on history and memory testing, which is often difficult and not accurate, as the early cognitive and behavioral symptoms of AD are difficult to distinguish from normal signs of aging. To facilitate the early diagnosis of this disease, there is an urgent need for the sensitive non-invasive detection of biomarkers for the pathophysiology. Toward achieving this goal, nuclear imaging techniques such as positron emission tomography (PET) and single photon emission computed tomography (SPECT) have been employed. Radionuclide-labeled agents targeting the Aβ plaques in the brain may greatly facilitate the diagnosis of AD [4,5].

Over recent years, great efforts have been put into developing Aβ imaging agents for PET, including 2-(4′-[$^{11}$C]methylaminophenyl)-6-hydroxybenzothiazole [6,7], "2-(4'-[$^{11}$C]methylaminophenyl)-6-hydroxybenzothiazole ([$^{11}$C]PIB)[6,7], 4-*N*-[$^{11}$C]methylamino-4'-hydroxystilbene ([$^{11}$C]SB-13)[8,9], [$^{11}$C]-2-(2-[2-dimethylaminothiazol-5-yl]ethenyl)-6-(2-[fluoro]ethoxy)benzoxazole ([$^{11}$C]BF-227) [10], [$^{18}$F]-2-(1-(2-(*N*-(2-fluoroethyl)-*N*-methylamino)-naphthalene-6-yl)ethylidene)malononitrile ([$^{18}$F]FDDNP)

* Corresponding authors. Masahiro Ono is to be contacted at Tel.: +81 75 753 4608; fax: +81 75 753 4568. Hideo Saji. Tel.: +81 75 753 4556; fax: +81 75 753 4568.
*E-mail addresses:* ono@pharm.kyoto-u.ac.jp (M. Ono), hsaji@pharm.kyoto-u.ac.jp (H. Saji).

0969-8051/$ – see front matter © 2011 Elsevier Inc. All rights reserved.
doi:10.1016/j.nucmedbio.2010.09.012

[11-13], [$^{18}$F]-4-(*N*-methylamino)-4'-(2-(2-(2-fluoroethoxy) ethoxy)ethoxy)-stilbene ([$^{18}$F]BAY94-9172)[14], and [$^{18}$F] -(*E*)-4-(2-(6-(2-(2-(2-fluoroethoxy)ethoxy)ethoxy)pyridin-3-yl)vinyl)-*N*-methylaniline ([$^{18}$F]AV-45)[15,16]2-(4'-[$^{11}$C] methylaminophenyl)-6-hydroxybenzothiazole [6,7] (Fig. 1). However, the development of imaging agents for SPECT is lagging far behind. Although some groups have reported radioiodinated ligands for Aβ plaques, unfavorable pharmacokinetics in vivo such as low uptake into the brain and a slow washout have prevented further development as imaging agents for SPECT [17–20]. [$^{123}$I]-6-iodo-2-(4′-dimethylamino-)phenyl-imidazo [1,2] pyridine ([$^{123}$I]IMPY, Fig. 1) is the first SPECT probe to be tested in humans. The preliminary clinical data showed a poor signal-to-noise ratio, making it difficult to distinguish AD patients, possibly due to high lipophilicity and low stability [21–23].

In an attempt to develop more practical Aβ imaging agents for SPECT with favorable pharmacokinetics in vivo, especially high signal-to-noise ratios, we have screened the structure of 2-phenyl-1H-benzo[*d*]imidazole (BZMZ) which is similar to IMPY. We reasoned that the active hydrogen in the imidazole ring would reduce the lipophilicity of the probes, thus reducing nonspecific binding and enhancing the signal-to-noise ratio. As expected, the calculated log D value of phenylbenzo[*d*]imidazole, 2.69, was lower than that of phenylimidazo[1,2-*a*]pyridine (4.21) (calculated with the Sparc On-Line Calculator). Here, we report the synthesis and biological evaluation of BZMZ derivatives as potential Aβ imaging agents for SPECT.

## 2. Methods and materials

### 2.1. General remarks

All the chemicals used were commercial products employed without further purification. The $^{1}$H-nuclear magnetic resonance (NMR) spectra were obtained at 400 MHz on JEOL JNM-AL400 NMR spectrometers in $CD_3OD$ solutions at room temperature with tetramethylsilane (TMS) as an internal standard. Chemical shifts are reported as δ values relative to the internal TMS. Coupling constants are reported in Hertz. Multiplicity is defined by s (singlet), d (doublet), t (triplet), and m (multiplet). Mass spectra were acquired with Shimadzu GC-MS-QP2010 Plus (ESI). High-performance liquid chromatography (HPLC) was performed with a Shimadzu system (a LC-10AT pump with a SPD-10A ultraviolet detector, λ=254 nm) using a column of Cosmosil C18 (Nakalai Tesque, 5$C_{18}$-AR-II, 4.6×150 mm) and acetonitrile/water (0.1% $Et_3N$) (50/50) as the mobile phase at a flow rate of 1.0 ml/min. Fluorescent observation was performed by microscope (Nikon Eclipse 80i) equipped with a BV-2A filter set (excitation, 400–440 nm; diachronic mirror, 455 nm; long pass filter, 470 nm). All key compounds were proven by this method to show ≥95% purity.

### 2.2. Chemistry

#### 2.2.1. 4-(6-Bromo-1H-benzo[d]imidazol-2-yl)-N,N-dimethylaniline (1)

A mixture of 4-bromobenzene-1,2-diamine (187 mg, 1.0 mmol), 4-(dimethylamino)benzaldehyde (149 mg, 1.0 mmol), and $Na_2S_2O_5$ (190 mg, 1.0 mmol) dissolved in 8 ml of dimethylformamide (DMF) was heated to reflux for 2 h. Ice water (50 ml) was added, and the precipitate formed was collected by filtration, washed with water and dried under vacuum to obtain 271 mg of **1** (85.8%). $^{1}$H NMR (400 MHz, $CD_3OD$) δ 8.00 (d, *J*=9.0 Hz, 2H), 7.76 (d, *J*=1.6 Hz, 1H), 7.53 (d, *J*=8.5 Hz, 1H), 7.39 (dd, *J*=8.5, 1.8 Hz, 1H), 6.88 (d, *J*=9.1 Hz, 2H), 3.04 (s, 6H). MS (ESI): *m/z* calcd for $C_{15}H_{14}BrN_3$ 315.04; found 316.00 ($M+H^+$).

#### 2.2.2. 6-Bromo-2-(4-nitrophenyl)-1H-benzo[d]imidazolo (2)

The same reaction described above to prepare **1** was used, and 282 mg of **2** was obtained in a yield of 88.7%. $^{1}$H NMR (400 MHz, $CD_3OD$) δ 8.57 (d, *J*=8.7 Hz, 2H), 7.91 (s, 1H), 7.30 (d, *J*=8.2 Hz, 1H), 7.14 (d, *J*=8.3 Hz, 1H), 6.69 (d, *J*=8.8 Hz, 2H). MS (ESI): *m/z* calcd for $C_{13}H_8BrN_3O_2$ 316.98; found 318.01 ($M+H^+$).

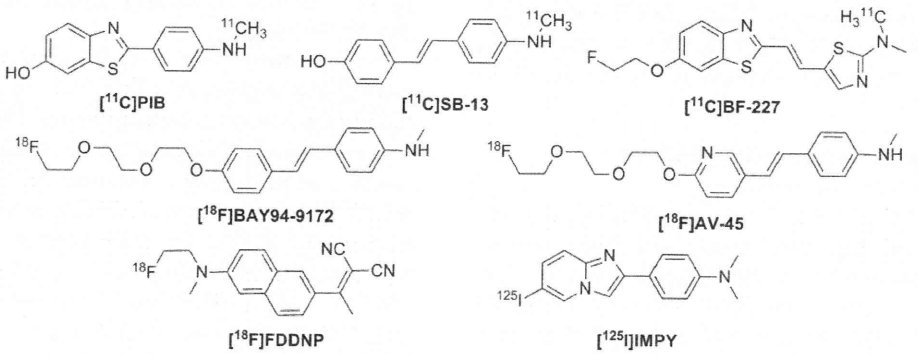


Fig. 1. Chemical structure of Aβ imaging probes in clinical trials.

*2.2.3. 6-Bromo-2-(4-methoxyphenyl)-1H-benzo[d]imidazole (3)*

The reaction described for **1** was used, and 246 mg of **3** was obtained in a yield of 81.2%. $^1$H NMR (400 MHz, $CD_3OD$) δ 8.01 (d, *J*=8.8 Hz, 2H), 7.71 (s, 1H), 7.47 (d, *J*=8.2 Hz, 1H), 7.34 (d, *J*=8.5 Hz, 1H), 7.09 (d, *J*=8.8 Hz, 2H), 3.88 (s, 3H). MS (ESI): *m/z* calcd for $C_{14}H_{11}BrN_2O$ 302.01; found 303.09 ($M+H^+$).

*2.2.4. 4-(6-Bromo-1H-benzo[d]imidazol-2-yl)phenol (4)*

The reaction described for **1** was used, and 247 mg of **4** was obtained in a yield of 85.3%. $^1$H NMR (400 MHz, $CD_3OD$) δ 7.93 (d, *J*=8.7 Hz, 2H), 7.73 (d, *J*=1.8 Hz, 1H), 7.50 (d, *J*=8.6 Hz, 1H), 7.38 (dd, *J*=8.6, 1.8 Hz, 1H), 6.95 (d, *J*=8.7 Hz, 2H). MS (ESI): *m/z* calcd for $C_{13}H_9BrN_2O$ 287.99; found 289.04 ($M+H^+$).

*2.2.5. 4-(6-Bromo-1H-benzo[d]imidazol-2-yl)aniline (5)*

A mixture of **2** (318 mg, 1.0 mmol) and $SnCl_2$ (380 mg, 2.0 mmol) dissolved in 50 ml of ethanol containing 2 ml of concentrated hydrochloric acid was stirred under reflux for 2 h. After the mixture had cooled to room temperature, 2 M NaOH (100 ml) was added and extracted with ethyl acetate (100 ml). The organic layer was dried over $Na_2SO_4$. The filtrate was concentrated to give 267 mg of **5** (92.7%).$^1$H NMR (400 MHz, $CD_3OD$) δ 7.80 (d, *J*=8.8 Hz, 2H), 7.65 (d, *J*=1.3 Hz, 1H), 7.41 (d, *J*=8.5 Hz, 1H), 7.29 (dd, *J*=8.5, 1.9 Hz, 1H), 6.78 (d, *J*=8.9 Hz, 2H). MS (ESI): *m/z* calcd for $C_{13}H_{10}BrN_3$ 287.01; found 288.00 ($M+H^+$).

*2.2.6. 4-(6-Bromo-1H-benzo[d]imidazol-2-yl)-N-methylaniline (6)*

A solution of $CH_3ONa$ (28 wt% in MeOH, 0.27 ml) was added dropwise to a mixture of **5** (288 mg, 1.0 mmol) and paraformaldehyde (104 mg, 4.0 mmol) in methanol (20 ml). The mixture was stirred under reflux for 1 h. After cooling, $NaBH_4$ (64 mg, 2.0 mmol) was added slowly, and the solution was heated under reflux for 2 h. 1 M NaOH (50 ml) was added to the cold mixture and extracted with $CHCl_3$ (30 ml). The organic phase was dried over $Na_2SO_4$ and filtered. The solvent was removed, and the residue was purified by silica gel chromatography (hexane:ethyl acetate=2:1) to give 194.2 mg of **6** (64.3%). $^1$H NMR (400 MHz, $CDCL_3$) δ 7.87 (d, *J*=8.6 Hz, 2H), 7.69 (s, 1H), 7.42 (s, 1H), 7.31 (dd, *J*=8.5, 1.7 Hz, 1H), 6.65 (d, *J*=8.7 Hz, 2H), 4.07 (s, 1H), 2.90 (s, 3H). MS (ESI): *m/z* calcd for $C_{14}H_{12}BrN_3$ 301.02; found 302.00 ($M+H^+$).

*2.2.7. N,N-Dimethyl-4-(6-(tributylstannyl)-1H-benzo[d]imidazol-2-yl)aniline (7)*

A mixture of **1** (126 mg, 0.4 mmol), $(Bu_3Sn)_2$ (0.4 ml) and $(Ph_3P)_4Pd$ (47 mg, 0.04 mmol) in a mixed solvent (10 ml, 1:1 dioxane/$Et_3N$) was stirred under reflux for 10 h. The solvent was removed, and the residue was purified by preparative NH TLC (hexane:ethyl acetate=2:1) to give 41 mg of **7** (19.3%). $^1$H NMR (400 MHz, $CD_3OD$) δ 7.92 (d, *J*=8.9 Hz, 2H), 7.63 (s, 1H), 7.52 (d, *J*=7.7 Hz, 1H), 7.24 (d, *J*=7.8 Hz, 1H), 6.81 (d, *J*=8.9 Hz, 2H), 3.00 (s, 6H), 1.68–0.89 (m, 27H). MS (ESI): *m/z* calcd for $C_{27}H_{41}N_3Sn$ 527.23; found 528.30 ($M+H^+$).

*2.2.8. N-Methyl-4-(6-(tributylstannyl)-1H-benzo[d]imidazol-2-yl)aniline (8)*

The reaction described for **7** was used, and 30 mg of **8** was obtained in a yield of 23.2%. $^1$H NMR (400 MHz, $CD_3OD$) δ 7.88 (d, *J*=7.7 Hz, 1H), 7.87 (d, *J*=8.8 Hz, 2H), 7.51 (s, 1H), 7.25 (d, *J*=7.8 Hz, 1H), 6.70 (d, *J*=8.8 Hz, 2H), 2.84 (s, 3H), 1.78–0.67 (m, 27H). MS (ESI): *m/z* calcd for $C_{26}H_{39}N_3Sn$ 513.22; found 514.29 ($M+H^+$).

*2.2.9. 4-(6-(Tributylstannyl)-1H-benzo[d]imidazol-2-yl)aniline (9)*

The reaction described for **7** was used, and 17 mg of **9** was obtained in a yield of 13.7%. $^1$H NMR (400 MHz, $CD_3OD$) δ 7.83 (d, *J*=8.7 Hz, 2H), 7.67 (s, 1H), 7.42 (d, *J*=7.8 Hz, 1H), 7.26 (d, *J*=7.8 Hz, 1H), 6.79 (d, *J*=8.6 Hz, 2H), 2.13–0.63 (m, 27H). MS (ESI): *m/z* calcd for $C_{25}H_{37}N_3Sn$ 498.29; found 499.33 ($M+H^+$).

*2.2.10. 2-(4-Methoxyphenyl)-6-(tributylstannyl)-1H-benzo[d]imidazole (10)*

The reaction described for **7** was used, and 35 mg of **10** was obtained in a yield of 27.2%. $^1$H NMR (400 MHz, $CD_3OD$) δ 8.03 (d, *J*=9.0 Hz, 2H), 7.68 (s, 1H), 7.57 (d, *J*=7.8 Hz, 1H), 7.29 (d, *J*=7.8 Hz, 1H), 7.08 (d, *J*=9.0 Hz, 2H), 3.88 (s, 3H), 1.73–0.79 (m, 27H). MS (ESI): *m/z* calcd for $C_{26}H_{38}N_2OSn$ 514.20; found 515.31 ($M+H^+$).

*2.2.11. 4-(6-(Tributylstannyl)-1H-benzo[d]imidazol-2-yl)phenol (11)*

The reaction described for **7** was used, and 36 mg of **11** was obtained in a yield of 29.1%. $^1$H NMR (400 MHz, $CD_3OD$) δ 7.94 (d, *J*=8.7 Hz, 2H), 7.66 (s, 1H), 7.55 (d, *J*=7.0 Hz, 1H), 7.28 (d, *J*=7.8 Hz, 1H), 6.93 (d, *J*=8.7 Hz, 2H), 1.64–0.88 (m, 27H). MS (ESI): *m/z* calcd for $C_{25}H_{36}N_2OSn$ 500.18; found 501.22 ($M+H^+$).

*2.2.12. 4-(6-Iodo-1H-benzo[d]imidazol-2-yl)-N,N-dimethylaniline (12)*

To a solution of **7** (53 mg, 0.1 mmol) in $CHCl_3$ (10 ml) was added a solution of iodine (127 mg dissolved in 10 ml $CHCl_3$) dropwise at room temperature. The resulting mixture was stirred at room temperature for 30 min and quenched by addition of 100 μl of a saturated $NaHSO_3$ solution. The organic phase was separated, dried over $MgSO_4$, filtered, and concentrated to give the crude product which was recrystallized in ethyl acetate to give 17 mg of **12** (46.8% yield). $^1$H NMR (400 MHz, $CD_3OD$) δ 7.95 (d, *J*=8.9 Hz, 2H), 7.90 (s, 1H), 7.51 (d, *J*=8.4 Hz, 1H), 7.36 (d, *J*=7.5 Hz, 1H), 6.88 (d, *J*=8.9 Hz, 2H), 3.08 (s, 6H). HRMS *m/z* ($EI^+$): calcd for $C_{15}H_{14}IN_3$ 363.0233; found 363.0228.

*2.2.13. 4-(6-Iodo-1H-benzo[d]imidazol-2-yl)-N-methylaniline (**13**)*

The reaction described for **12** was used, and 8 mg of **13** was obtained in a yield of 39.1%. $^1$H NMR (400 MHz, $CD_3OD$) δ 7.96 (s, 1H), 7.86 (d, *J*=8.7 Hz, 2H), 7.67 (d, *J*=8.5 Hz, 1H), 7.41 (d, *J*=8.4 Hz, 1H), 6.75 (d, *J*=8.7 Hz, 2H), 2.87 (s, 3H). HRMS *m/z* ($EI^+$): calcd for $C_{14}H_{12}IN_3$ 349.0076; found 349.0081.

*2.2.14. 4-(6-Iodo-1H-benzo[d]imidazol-2-yl)aniline (**14**)*

The reaction described for **12** was used, and 11 mg of **14** was obtained in a yield of 27.6%. $^1$H NMR (400 MHz, $CD_3OD$) δ 7.81 (d, *J*=8.6 Hz, 2H), 7.76 (s, 1H), 7.50 (d, *J*=9.4 Hz, 1H), 7.38 (d, *J*=8.6 Hz, 1H), 6.81 (d, *J*=8.6 Hz, 2H). HRMS *m/z* ($EI^+$): calcd for $C_{13}H_{10}IN_3$ 334.9920; found 334.9923.

*2.2.15. 6-Iodo-2-(4-methoxyphenyl)-1H-benzo[d]imidazolo (**15**)*

The reaction described for **12** was used, and 19 mg of **15** was obtained in a yield of 41.5%. $^1$H NMR (400 MHz, $CD_3OD$) δ 8.01 (d, *J*=8.9 Hz, 2H), 7.91 (s, 1H), 7.52 (dd, *J*=8.4, 1.6 Hz, 1H), 7.37 (d, *J*=8.4 Hz, 1H), 7.09 (d, *J*=8.9 Hz, 2H), 3.88 (s, 3H). HRMS *m/z* ($EI^+$): calcd for $C_{14}H_{11}IN_2O$ 349.9916; found 349.9909.

*2.2.16. 4-(6-Iodo-1H-benzo[d]imidazol-2-yl) phenol (**16**)*

The reaction described for **12** was used, and 22 mg of **16** was obtained in a yield of 29.7%. $^1$H NMR (400 MHz, $CD_3OD$) δ 7.92 (d, *J*=8.7 Hz, 2H), 7.90 (s, 1H), 7.51 (d, *J*=8.5 Hz, 1H), 7.36 (d, *J*=7.5 Hz, 1H), 6.93 (d, *J*=8.7 Hz, 2H). HRMS *m/z* ($EI^+$): calcd for $C_{13}H_9IN_2O$ 335.9760; found 335.9764.

*2.3. Radiolabeling*

The radioiodinated ligand [$^{125}$I]**12** was prepared from the corresponding tributyltin precursor through an iododestannylation reaction according to a procedure described previously with some modifications [21]. Briefly, 50 μl of $H_2O_2$ (3%) was added to a mixture of a tributyltin derivative (0.1 mg/100 μl in ethanol), 200 μCi of sodium [$^{125}$I]iodide (specific activity 2200 Ci/mmol), and 100 μl of 1 M HCl in a sealed vial. The reaction was allowed to proceed at room temperature for 15 min and then quenched with the addition of 50 μl of a saturated $NaHSO_3$ solution. The reaction mixture was extracted with ethyl acetate (3×1 ml) after neutralization with 10 mg of sodium bicarbonate. The combined extracts were evaporated dry. The residues were dissolved in 100 μl of EtOH and purified by HPLC using a 5$C_{18}$-AR-II analytical column (4.6×150 mm) with an isocratic solvent, $CH_3CN/H_2O$ (0.1% $Et_3N$)=1/1, at a flow rate of 1.0 ml /min. The desired fractions containing the product were evaporated dry and redissolved in 100% ethanol. Finally, the radiochemical identity of [$^{125}$I]**12** was verified by coinjection with nonradioactive compound by HPLC. The final product was stored at −20°C for autoradiography and biodistribution experiments.

*2.4. Binding assay in vitro using Aβ Aggregates*

Inhibition experiments were carried out in 12×75 mm borosilicate glass tubes according to a procedure described previously with some modifications [17]. One hundred microliters of aggregated Aβ fibrils (60 nM in the final assay mixture) was added to a mixture containing 100 μl of radioligand ([$^{125}$I]IMPY) of the appropriate concentration, 10 μl of inhibitor ($10^{-5}$–$10^{-10}$ M in ethanol) and 790 μl of phosphate-buffered saline (PBS) (0.2 M, pH=7.4) in a final volume of 1 ml. Nonspecific binding was defined in the presence of 1 μM IMPY. The mixture was incubated for 2 h at 37°C with constant shaking, then the bound and free radioactivity were separated by vacuum filtration through borosilicate glass fiber filters (Whatman GF/B) using a M-24 cell harvester (Brandel, Gaithersburg, MD, USA). Filters containing the bound $^{125}$I ligand were measured for radioactivity in a γ-counter (WALLAC/Wizard 1470, PerkinElmer, Boston, MA, USA) with 70% counting efficiency. Under the assay conditions, the specifically bound fraction accounted for about 10% of all the radioactivity. The half maximal inhibitory concentration ($IC_{50}$) was determined using GraphPad Prism 4.0, and those for the inhibition constant ($K_i$) was calculated using the Cheng-Prusoff equation: $K_i=IC_{50}/(1+[L]/K_d)$ [24] (Table 1).

*2.5. Autoradiography in vitro using human brain sections*

Paraffin-embedded postmortem brain sections (Temporal lobe) of an AD patient (75-year-old male) and a control subject (20-year-old male) were obtained from BioChain. The sections were deparaffinized with 2×20-min washes in xylene, 2×5-min washes in 100% ethanol, a 5-min wash in 90% ethanol/$H_2O$, a 5-min wash in 80% ethanol/$H_2O$, a 5-min wash in 60% ethanol/$H_2O$ and a 10-min wash in running tap water and then incubated in PBS (0.2 M, pH=7.4) for 30 min. The sections were incubated with [$^{125}$I]**12** (0.4 nM) for 1 h at room temperature. They were then washed with 40% ethanol for 3 min and rinsed with water for 30 s. After drying, the $^{125}$I-labeled sections were exposed to a Fuji Film imaging plate overnight. The in vitro autoradiographic images were obtained using a BAS5000 scanner system (Fuji Film). The presence and location of plaques in the sections were confirmed with immunohistochemical staining using a monoclonal Aβ antibody, BC05 (Wako) [25].

Table 1
Inhibition constants ($K_i$) for binding to aggregates of $A\beta_{1-42}$ versus [$^{125}$I]IMPY

| Compounds | $K_i$ (nM) |
|---|---|
| **12** | 9.8±1.2 |
| **13** | 40.3±4.5 |
| **14** | 315.1±11.2 |
| **15** | 190.1±6.4 |
| **16** | 901.5±22.1 |
| IMPY | 10.5±1.0 |

### 2.6. Autoradiography of [$^{125}$I]**12** ex vivo using AD model mice

Autoradiography was performed using Tg2576 transgenic (female, 22 months old) and wild-type (female, 22 months old) mice. A saline solution (100 μl, 5% EtOH) of 90 μCi of [$^{125}$I]**12** was injected intravenously through the femoral vein, and the animals were sacrificed by decapitation 2 hours later. The brains were removed and frozen in powdered dry ice immediately. Sections of 20 μm were cut and exposed to a BAS imaging plate (Fuji Film, Tokyo, Japan) for 70 h. Autoradiographic images were obtained using a BAS5000 scanner system (Fuji Film). After the autoradiographic examination, the presence of amyloid plaques was confirmed by staining the same sections with thioflavin-S in vitro. For the staining, the sections were immersed in a 0.125% solution of thioflavin-S containing 40% ethanol for 10 min and washed with 50% ethanol. After drying, fluorescent observation was performed by microscope (Nikon Eclipse 80i) with a BV-2A filter set (excitation, 400–440 nm; diachronic mirror, 455 nm; long-pass filter, 470 nm).

### 2.7. Biodistribution experiments with normal mice

The biodistribution experiments were performed in normal female ddY mice (average weight, about 20 g) and approved by the animal care committee of Kyoto University. A saline solution (100 μl, 5% EtOH) containing [$^{125}$I]**12** (1 μCi) was injected directly into the tail vein. The mice were sacrificed at various time points post-injection. The organs of interest were removed and weighed, and the radioactivity was measured with an automatic γ-counter (WALLAC/Wizard 1470, PerkinElmer, Boston, MA, USA). The percent dose per gram of wet tissue was calculated by a comparison of the tissue counts to suitably diluted aliquots of the injected material.

### 2.8. Determination of the partition coefficient

The partition coefficient of [$^{125}$I]**12** was determined as described previously but with some modifications [26]. [$^{125}$I]**12** (10 μCi) was added to premixed suspensions containing 3 g of *n*-octanol and 3 g of PBS (0.05 M, pH=7.4) in a test tube. The test tube was vortexed for 3 min at room temperature, and centrifuged for 5 min at 3000 rpm. Two weighted samples from the *n*-octanol (50 μl) and buffer (800 μl) layers were measured. The partition coefficient was expressed as the logarithm of the ratio of the counts per gram from *n*-octanol versus PBS. Samples from the *n*-octanol layer were repartitioned until consistent partitions of coefficient values were obtained. The measurement was done in triplicate and repeated three times.

## 3. Results and discussion

The synthesis of the BZMZ derivatives is outlined in Scheme 1. Compounds **1**, **2**, **3** and **4** were obtained by intermolecular cyclization between 4-bromobenzene-1,2-diamine and substituted benzaldehydes using $Na_2S_2O_5$ as an oxidant (yield, 81.2–88.7%). The monomethylamino derivative, **6**, was produced by first reducing the nitro group to an amino group with $SnCl_2$, and subsequent monomethylation of the amino group using paraformaldehyde, sodium borohydride, and sodium methoxide (yield, 64.3%). The tributyltin precursors (**7**–**11**) were prepared from the corresponding bromo compounds under a bromo to tributyltin exchange reaction catalyzed by $Pd(PPh_3)_4$ (yield, 13.7–29.1%). The tributyltin derivatives were readily reacted with iodine in $CHCl_3$ at room temperature to give the iodinated derivatives (**12**–**16**) with moderate yields (26.7–46.8%) [18].

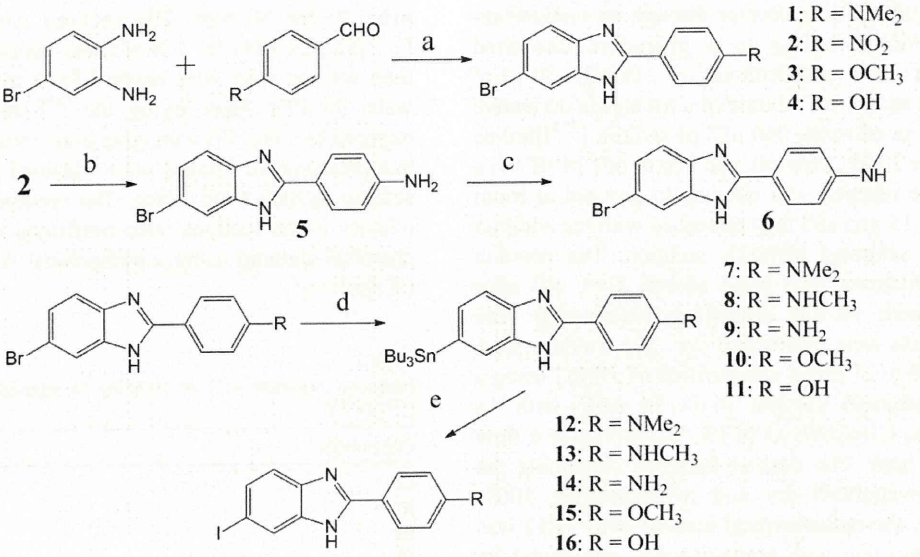


Scheme 1. Reagents and conditions: (a) $Na_2S_2O_5$, DMF, reflux; (b) $SnCl_2 \cdot 2H_2O$, EtOH, HCl, reflux; (c) MeOH, NaOMe, $(CH_2O)n$, $NaBH_4$; (d) $(Bu_3Sn)_2$, $(PPh_3)_4Pd$, dioxiane, $Et_3N$; (e) $I_2$, $CHCl_3$.

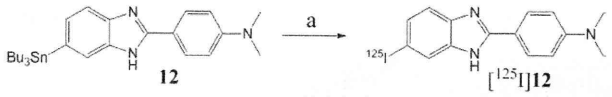


Scheme 2. Reagents and conditions: (a) [$^{125}$I]NaI, HCl (1N), $H_2O_2$ (3%).

The affinity of these nonradioactive derivatives (**12–16**) for $A\beta_{1-42}$ aggregates was examined with competition binding assays using [$^{125}$I]IMPY as the competing radioligand. IMPY was also screened using the same system for comparison (Table 1). Consistent with previous data on tertiary and secondary amino analogues of IMPY [27], the tertiary *N*,*N*-dimethylamino analogue **12** had higher affinity ($K_i$=9.8 nM, comparable to the value for IMPY) than the secondary methylamino analogue **13**, while the corresponding primary amino analogue **14** showed a much lower affinity. Comparing **15** with **16**, substitution of the methoxy group with the hydroxy group decreased the binding. It is generally accepted that compounds containing electron donating groups show greater affinity [5,28]. For these BZMZ derivatives, the $K_i$ values decreased in the order of **16** (OH)>**14**($NH_2$)>**15** (OMe)>**13** (NHMe)>**12** ($NMe_2$), consistent with the order of increasing electron donating capacity.

On the basis of the binding data for these series of compounds, the tertiary *N*,*N*-dimethylamino analogue (**12**), which exhibits the highest affinity, was selected for further biological evaluation. The radioiodinated ligand, [$^{125}$I]**12**, was prepared from the corresponding tributyltin precursors through an iododestannylation reaction using hydrogen peroxide as an oxidant with a radiochemical yield of 43.2% (Scheme 2). After purification by HPLC, the radiochemical purity of this radiotracer was greater than 98%. The specific activity of the no-carrier-added preparation was comparable to that of Na$^{125}$I, 2200 Ci/mmol. Finally, the radiochemical identity of [$^{125}$I]**12** was verified by coinjection with a nonradioactive compound from HPLC profiles (see supporting information). [$^{125}$I]**12** showed moderate lipophilicity (log*D*=2.8) under the experimental conditions, which is desirable for penetrating the blood-brain barrier (BBB).

A biodistribution experiment in normal mice injected intravenously showed that [$^{125}$I]**12** exhibited good initial penetration of the BBB with excellent initial uptake in the brain [4.14 percent injected dose per gram (% ID/g) at 2 min]. Because there are no plaques to cause the retention of Aβ-specific probes, the high uptake of [$^{125}$I]**12** was subsequently followed by a fast washout, with 0.15% ID/g remaining in the brain at 60 min (Table 2). The brain uptake of [$^{125}$I]**12** was similar to that of [$^{125}$I]IMPY under the same experimental conditions (4.8% ID/g at 2 min and 0.36% ID/g at 1 h post-injection). However, the washout rate (the ratio of the brain uptake at 2 min to that of 60 min) was 28, which is higher than [$^{125}$I]IMPY. The failure of [$^{123}$I]IMPY in humans could be due to low specific binding signal as well as high background which lead to a poor signal-to-noise ratio. A high initial uptake in normal mouse brain coupled with a fast washout rate of the radioiodinated tracer [$^{125}$I]**12** are highly desirable properties for Aβ imaging agents, which may bring about a good signal-to-noise ratio and therefore achieve highly sensitive detection.

To further characterize the nature of the binding to Aβ plaques, autoradiography was performed by incubating [$^{125}$I]**12** with sections of AD and control brains. As shown in Fig. 2A, [$^{125}$I]**12** displayed excellent labeling with a strong signal and a low background in AD brain sections, but not control sections (Fig. 2C). Furthermore, the hot spots of radioactivity were consistent with the results of in vitro immunohistochemical staining in the same sections (Fig. 2B). The results confirm the binding of [$^{125}$I]**12** to Aβ plaques in the brain of AD patients.

To test the labeling of plaques in vivo, [$^{125}$I]**12** was injected intravenously into 22-month-old transgenic model (APPswTg2576) mice, which were expected to produce excess amyloid plaques in the brain, and age-matched control mice. Two hours after the injection, the brains were removed, frozen and sectioned for autoradiography. Compared with control mice (Fig. 3B), the transgenic mice showed dense labeling of plaques in the cortical regions and

Table 2
Biodistribution of [$^{125}$I]**12** in normal mice (% ID/g, mean±S.D., n=4)

| Organ | 2 min | 10 min | 30 min | 60 min | 120 min |
|---|---|---|---|---|---|
| Blood | 6.93±0.92 | 3.84±0.35 | 1.90±0.17 | 0.97±0.15 | 0.84±0.10 |
| Brain | 4.14±0.24 | 1.59±0.09 | 0.43±0.03 | 0.15±0.01 | 0.08±0.01 |
| Heart | 3.75±2.19 | 2.38±0.04 | 1.00±0.06 | 0.47±0.06 | 0.36±0.05 |
| Liver | 27.20±2.79 | 28.76±3.31 | 15.71±3.65 | 10.03±0.89 | 8.08±3.54 |
| Spleen | 5.37±0.33 | 3.61±0.38 | 1.33±0.15 | 0.71±0.07 | 0.55±0.06 |
| Lung | 7.83±0.63 | 4.18±0.54 | 2.10±0.38 | 1.05±0.10 | 0.89±0.20 |
| Kidney | 11.94±1.23 | 8.47±0.59 | 4.87±1.31 | 1.67±0.70 | 1.16±0.12 |
| Stomach[a] | 2.08±0.42 | 5.70±1.01 | 7.44±2.38 | 8.25±1.94 | 4.27±2.39 |
| Intestine | 3.53±0.64 | 17.46±1.95 | 29.75±1.99 | 40.98±5.47 | 40.83±4.79 |

[a] Expressed as % ID/g.

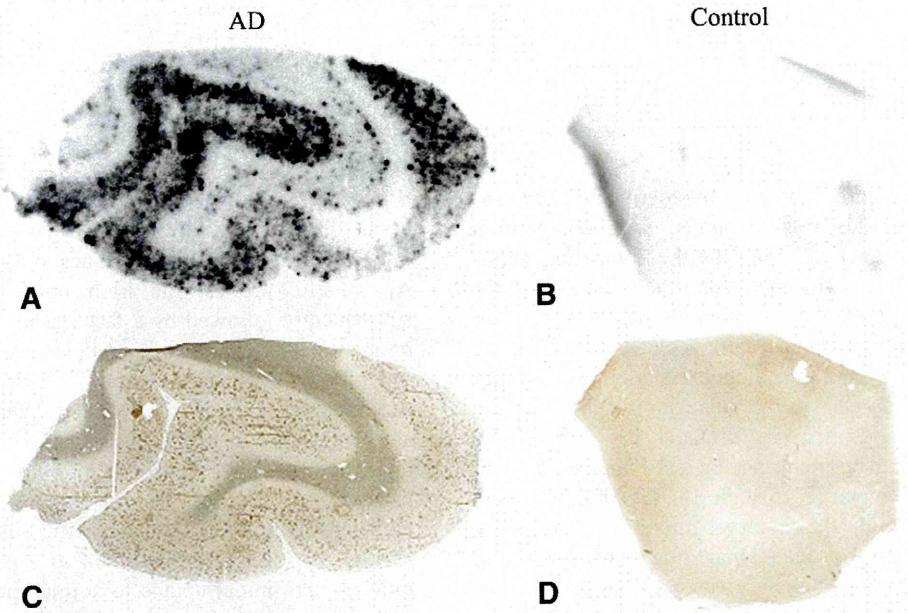


Fig. 2. Autoradiography of [$^{125}$I]**12** in vitro in AD brain sections and control sections (Temporal lobe) (A and B). The presence and distribution of plaques in the sections were confirmed with immunohistochemical staining using a monoclonal Aβ antibody (C and D).

hippocampus with low background images (Fig. 3A). Furthermore, the plaques labeled with [$^{125}$I]**12** showed a one-to-one correlation with the fluorescent signals obtained with thioflavin-S (Fig. 3C). The result was comparable to that reported for [$^{125}$I]IMPY [21].

## 4. Conclusion

In conclusion, we have demonstrated that iodinated 2-phenyl-1H-benzo[*d*]imidazole derivatives can be successfully synthesized. The compound with a *N*,*N*-dimethylamino

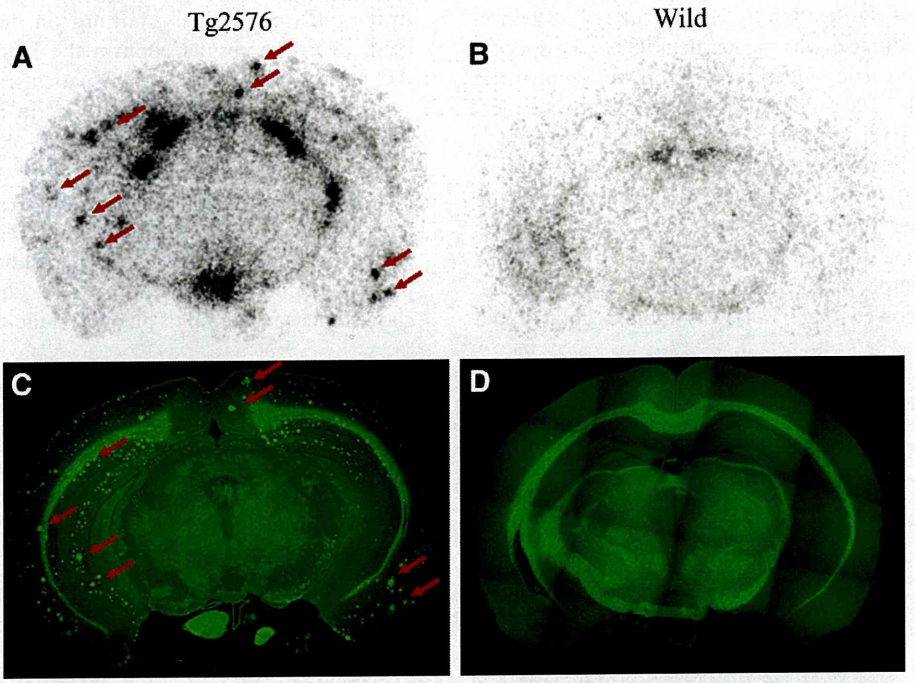


Fig. 3. Autoradiography of [$^{125}$I]**12** ex vivo using 22-month-old transgenic (APPswTg2576) mice and wild-type controls (A and B). Plaques were also confirmed by the staining of the same sections with thioflavin-S in vitro (C and D). Arrows show plaques labeled by [$^{125}$I]**12** and thioflavin-S.

moiety showed high affinity for Aβ aggregates in assays in vitro. The radioiodinated derivative [$^{125}$I]**12** displayed excellent uptake into and rapid washout from the brain after its injection in normal mice. Specific labeling of Aβ plaques was demonstrated by autoradiography with AD brain sections in vitro and autoradiograms of transgenic mice in vivo. These findings suggest that **12** is a promising SPECT probe for the imaging of amyloid plaques in the brain when labeled with iodine-123.

## Acknowledgments

This study was supported by the Program for Promotion of Fundamental Studies in Health Sciences of the National Institute of Biomedical Innovation (NIBIO), a Health Labour Sciences Research Grant, and a Grant-in-aid for Young Scientists (A) and Exploratory Research from the Ministry of Education, Culture, Sports, Science and Technology, Japan. This study was also supported by the China Scholarship Council (CSC).

## References

[1] Hardy JA, Higgins GA. Alzheimer's disease: the amyloid cascade hypothesis. Science 1992;256:184–5.
[2] Selkoe DJ. The origins of Alzheimer disease: A is for amyloid. JAMA 2000;283:1615–7.
[3] Hardy JA, Selkoe DJ. The amyloid hypothesis of Alzheimer's disease: progress and problems on the road to therapeutics. Science 2002;297: 353–6.
[4] Mathis CA, Wang Y, Klunk WE. Imaging β-amyloid plaques and neurofibrillary tangles in the aging human brain. Curr Pharm Des 2004;10:1469–92.
[5] Cai LS, Innis RB, Pike VW. Radioligand development for PET imaging of β-amyloid (Aβ)-current status. Curr Med Chem 2007;14: 19–52.
[6] Klunk WE, Engler H, Nordberg A, Wang Y, Blomqvist G, Holt DP, et al. Imaging brain amyloid in Alzheimer's disease with Pittsburgh compound-B. Ann Neurol 2004;55:306–19.
[7] Mathis CA, Wang Y, Holt DP, Huang GF, Debnath ML, Klunk WE. Synthesis and evaluation of $^{11}$C-labeled 6-substituted 2-arylbenzothiazoles as amyloid imaging agents. J Med Chem 2003;46:2740–54.
[8] Verhoeff NP, Wilson AA, Takeshita S, Trop L, Hussey D, Singh K, et al. In vivo imaging of Alzheimer disease β-amyloid with [$^{11}$C]SB-13 PET. Am J Geriatr Psychiatry 2004;12:584–95.
[9] Ono M, Wilson A, Nobrega J, Westaway D, Verhoeff P, Zhuang ZP, et al. $^{11}$C-Labeled stilbene derivatives as Aβ-aggregate-specific PET imaging agents for Alzheimer's disease. Nucl Med Biol 2003;30: 565–71.
[10] Kudo Y, Okamura N, Furumoto S, Tashiro M, Furukawa K, Maruyama M, et al. 2-(2-[2-Dimethylaminothiazol-5-yl]ethenyl)-6-(2-[fluoro]ethoxy)benzoxazole: a novel PET agent for in vivo detection of dense amyloid plaques in Alzheimer's disease patients. J Nucl Med 2007;48:553–6.
[11] Agdeppa ED, Kepe V, Liu J, Flores-Torres S, Satyamurthy N, Petric A, et al. Binding characteristics of radiofluorinated 6-dialkylamino-2-naphthylethylidene derivatives as positron emission tomography imaging probes for β-amyloid plaques in Alzheimer's disease. J Neurosci 2001;21:RC189.
[12] Shoghi-Jadid K, Small GW, Agdeppa ED, Kepe V, Ercoli LM, Siddarth P, et al. Localization of neurofibrillary tangles and β-amyloid plaques in the brains of living patients with Alzheimer disease. Am J Geriatr Psychiatry 2002;10:24–35.
[13] Small GW, Kepe V, Ercoli LM, Siddarth P, Bookheimer SY, Miller KJ, et al. PET of brain amyloid and tau in mild cognitive impairment. N Engl J Med 2006;355:2652–63.
[14] Rowe CC, Ackerman U, Browne W, Mulligan R, Pike KL, O'Keefe G, et al. Imaging of amyloid β in Alzheimer's disease with 18F-BAY94-9172, a novel PET tracer: proof of mechanism. Lancet Neurol 2008;7: 129–35.
[15] Choi SR, Golding G, Zhuang ZP, Zhang W, Lim N, Hefti F, et al. Preclinical properties of 18F-AV-45: a PET agent for Aβ plaques in the brain. J Nucl Med 2009;50:1887–94.
[16] Kung HF, Choi SR, Qu WC, Zhang W, Skovronsky D. 18F Stilbenes and styrylpyridines for PET imaging of Aβ plaques in Alzheimer's disease: a miniperspective. J Med Chem 2010;53:933–41.
[17] Zhuang ZP, Kung MP, Hou C, Skovronsky DM, Gur TL, Plossl K, et al. Radioiodinated styrylbenzenes and thioflavins as probes for amyloid aggregates. J Med Chem 2001;44:1905–14.
[18] Ono M, Kung MP, Hou C, Kung HF. Benzofuran derivatives as Aβ-aggregate-specific imaging agents for Alzheimer's disease. Nucl Med Biol 2002;29:633–42.
[19] Zhuang ZP, Kung MP, Hou C, Plossl K, Skovronsky D, Gur TL, et al. IBOX(2-(4′-dimethylaminophenyl)-6-iodobenzoxazole): a ligand for imaging amyloid plaques in the brain. Nucl Med Biol 2001;28: 887–94.
[20] Qu WC, Kung MP, Hou C, Benedum TE, Kung HF. Novel styrylpyridines as probes for SPECT imaging of amyloid plaques. J Med Chem 2007;50:2157–65.
[21] Kung MP, Hou C, Zhuang ZP, Zhang B, Skovronsky D, Trojanowski JQ, et al. IMPY: an improved thioflavin-T derivative for in vivo labeling of beta-amyloid plaques. Brain Res 2002;956:202–10.
[22] Zhuang ZP, Kung MP, Wilson A, Lee CW, Plossl K, Hou C, et al. Structure-activity relationship of imidazo[1,2-a]pyridines as ligands for detecting β-amyloid plaques in the brain. J Med Chem 2003;46: 237–43.
[23] Newberg AB, Wintering NA, Plossl K, Hochold J, Stabin MG, Watson M, et al. Safety, biodistribution, and dosimetry of $^{123}$I-IMPY: a novel amyloid plague-imaging agent for the diagnosis of Alzheimer's disease. J Nucl Med 2006;47:748–54.
[24] Cheng Y, Prusoff W. Biochem Pharmacol 1973;1973:3099.
[25] Maya Y, Ono M, Watanabe H, Haratake M, Saji H, Nakayama M. Novel radioiodinated aurones as probes for SPECT imaging of β-amyloid plaques in the brain. Bioconjugate Chem 2009;20:95–101.
[26] Wu CY, Wei JJ, Gao KQ, Wang YM. Dibenzothiazoles as novel amyloid-imaging agents. Bioorg Med Chem 2007;15:2789–96.
[27] Cai LS, Cuevas J, Temme S, Herman MM, Dagostin C, Widdowson DA, et al. Synthesis and structure affinity relationships of new 4-(6-Iodo-H-imidazo[1,2-a]pyridin-2-yl)-*N*-dimethylbenzeneamine derivatives as ligands for human β-amyloid plaques. J Med Chem 2007;50: 4746–58.
[28] Kung HF, Lee CW, Zhuang ZP, Kung MP, Hou C, Plossl K. Novel stilbenes as probes for amyloid plaques. J Am Chem Soc 2001;123: 12740–1.

Neuroscience Letters 495 (2011) 210–215

Contents lists available at ScienceDirect

Neuroscience Letters

journal homepage: www.elsevier.com/locate/neulet

# Gene and protein analysis of brain derived neurotrophic factor expression in relation to neurological recovery induced by an enriched environment in a rat stroke model

Kenji Hirata[a], Yuji Kuge[b,*], Chiaki Yokota[c], Akina Harada[d], Koichi Kokame[e], Hiroyasu Inoue[f], Hidekazu Kawashima[d], Hiroko Hanzawa[g], Yuji Shono[c], Hideo Saji[d], Kazuo Minematsu[c], Nagara Tamaki[a,b]

[a] Department of Nuclear Medicine, Graduate School of Medicine, Hokkaido University, Japan
[b] Central Institute of Isotope Science, Hokkaido University, Japan
[c] Department of Cerebrovascular Medicine, National Cerebral and Cardiovascular Center, Japan
[d] Department of Patho-Functional Bioanalysis, Graduate School of Pharmaceutical Sciences, Kyoto University, Japan
[e] Department of Molecular Pathogenesis, National Cerebral and Cardiovascular Center, Japan
[f] Department of Food Science and Nutrition, Nara Women's University, Japan
[g] Central Research Laboratory, Hitachi, Ltd., Japan

ARTICLE INFO

*Article history:*
Received 22 October 2010
Received in revised form 7 March 2011
Accepted 22 March 2011

*Keywords:*
Focal ischemia
Enriched environment
Brain derived neurotrophic factor

ABSTRACT

Although an enriched environment enhances functional recovery after ischemic stroke, the mechanism underlying this effect remains unclear. We previously reported that brain derived neurotrophic factor (BDNF) gene expression decreased in rats housed in an enriched environment for 4 weeks compared to those housed in a standard cage for the same period. To further clarify the relationship between the decrease in BDNF and functional recovery, we investigated the effects of differential 2-week housing conditions on the mRNA of BDNF and protein levels of proBDNF and mature BDNF (matBDNF). After transient occlusion of the right middle cerebral artery of male Sprague–Dawley rats, we divided the rats into two groups: (1) an enriched group housed multiply in large cages equipped with toys, and (2) a standard group housed alone in small cages without toys. Behavioral tests before and after 2-week differential housing showed better neurological recovery in the enriched group than in the standard group. Synaptophysin immunostaining demonstrated that the density of synapses in the peri-infarct area was increased in the enriched group compared to the standard group, while infarct volumes were not significantly different. Real-time reverse transcription polymerase chain reaction, Western blotting and immunostaining all revealed no significant difference between the groups. The present results suggest that functional recovery cannot be ascribed to an increase in matBDNF or a decrease in proBDNF but rather to other underlying mechanisms.



Functional impairment caused by stroke is a highly serious health problem throughout the world. Rehabilitation has been widely applied and has been shown to contribute greatly to neurological recovery. However, the mechanisms of the beneficial effects of rehabilitation remain unclear [3]. An enriched environment is a model of rehabilitation for rodents, in which multiple animals are housed together in a large cage equipped with toys. Enriched environments have been shown to enhance the recovery of neurological function impaired by experimental focal ischemia [13]. Brain-derived neurotrophic factor (BDNF), one of the neurotrophins, may be a key molecule in this effect, since it is central to many facets of the neural network, from differentiation and neuronal survival to synaptogenesis and activity-dependent forms of synaptic plasticity [9]. While an enriched environment increases BDNF expression in non-ischemic healthy animals [5], this is not the case with ischemic animals. The alteration of BDNF after ischemic stroke is not fully understood, although BDNF expression has been investigated in association with an enriched environment after experimental stroke. Zhao et al. demonstrated that BDNF mRNA

*Abbreviations:* BDNF, brain derived neurotrophic factor; GFAP, glial fibrillary acidic protein; GAPDH, glyceraldehyde 3-phosphate dehydrogenase; IPT, inclined plane test; MAP-2, microtubular-associated protein 2; matBDNF, mature BDNF; MCA, middle cerebral artery; NSS, neurological severity scores; ROI, region of interest; RT-PCR, reverse transcription polymerase chain reaction; SYP, synaptophysin; tMCAO, transient MCA occlusion.

* Corresponding author at: Central Institute of Isotope Science, Hokkaido University, Kita 15, Nishi 7, Kita-ku, Sapporo, Hokkaido 060-0815, Japan.
Tel.: +81 11 706 6087; fax: +81 11 706 7862.
*E-mail address:* kuge@ric.hokudai.ac.jp (Y. Kuge).

0304-3940/$ – see front matter © 2011 Elsevier Ireland Ltd. All rights reserved.
doi:10.1016/j.neulet.2011.03.068

[19] and BDNF protein [20] were decreased after ischemic stroke and housing in an enriched environment. Nygren et al. reported that BDNF +/− mice, which express low levels of BDNF, showed better stroke recovery in an enriched environment than their wild-type counterparts [12]. On the other hand, Risedal et al. observed no significant change of BDNF mRNA between rats in an enriched environment and those in a standard environment in their experiments using a permanent occlusion model [15]. In our previous investigation, microarray analysis and real-time reverse transcription polymerase chain reaction (RT-PCR) revealed a significant decrease in expression of the BDNF gene in the contralateral cortex to ischemia in rats in 4-week enriched environment [16]. Generally, BDNF is a beneficial molecule for neurons and neurological functions, and there thus appears to be a discrepancy between the decreased BDNF and improved neurological functions in these studies. There are at least two possible explanations for this phenomenon. The first one is that BDNF may be down-regulated, since the functionally improved brain may no longer need elevated BDNF after 4-week enrichment. Another possibility is that BDNF itself is an exacerbating factor for neurological deficit, especially in the post-stroke state, and that an enriched environment may eliminate BDNF to avoid its potentially deleterious effects. To examine these hypotheses, it will be necessary to examine brain tissue at an earlier time point when functional recovery has not been completed. Furthermore, proBDNF, a precursor of the BDNF protein, must be investigated, since it negatively influences neurons [9]. Thus, the objective of the present study was to investigate the expression of BDNF in rats subjected to focal cerebral ischemia followed by housing for 2 weeks in an enriched environment by using RT-PCR, Western blotting, and immunohistochemical techniques.

Nine-week-old, male Sprague–Dawley rats were anesthetized by chloral hydrate and the right middle cerebral artery (MCA) was occluded intraluminally for 60 min with nylon monofilaments, as previously described [8]. At 72–96 h after transient MCA occlusion (tMCAO), the rats were randomly divided into two groups, an enriched group and a standard group. For the enriched group, 4–6 rats were housed together in a large cage (610 mm × 460 mm × 460 mm) containing toys including a running wheel, a tunnel, balls, logs and rings, rearranged twice a week. For the standard group, rats were housed alone in a standard-sized cage (320 mm × 210 mm × 130 mm) containing food and water.

Ischemic animals were subjected to two behavioral tests, the neurological severity score test (NSS) [2] and the inclined plane test (IPT) [6]. These tests were performed 3 times, once before tMCAO, once at 3 or 4 days after tMCAO (defined as day 0), and once at 14 days after initiation of differential housing (defined as day 14). The NSS is a composite of motor, sensory, reflex, and balance tests. The score ranges from 0 to 18, with the higher score indicating severe neurological impairment. In this study, we analyzed rats that scored between 7 and 12 in the second test (day 0). The recovery rate was defined as $(NSS_{2nd} - NSS_{3rd})/NSS_{2nd}$. The IPT was performed to evaluate motor deficits. Each rat was placed up-headed or right-headed on a stainless steel plane steepening at a rate of $2^\circ\,s^{-1}$, and we recorded the angle when the rat slipped on the plate. The improvement index was calculated as $(IPT_{3rd} - IPT_{2nd})/(IPT_{1st} - IPT_{2nd})$. After the behavioral tests on day 14, rats were sacrificed and the brains were cut into 3 coronal sections with a thickness of 3 mm from the frontal pole.

The second blocks from the frontal pole were embedded in paraffin for the histological study. Microtubular-associated protein 2 (MAP-2), glial fibrillary acidic protein (GFAP), synaptophysin (SYP), and matBDNF were immunohistochemically stained. The infarct volume was calculated as $(C - I)/C$, where $C$ represents MAP-2-stained volume in contralateral side, and $I$ represents MAP-2-stained volume in ischemic side. To set regions of interest in peri-infarct area, we assessed both neuronal viability using MAP-2 staining and glial activity using GFAP staining. MAP-2 mainly distinguishes infarct area from non-infarct area, and GFAP mainly distinguishes peri-infarct area and distant intact area. The area with both preserved MAP-2 staining and intense GFAP staining was defined as peri-infarct area. SYP and BDNF immunoreactivity was quantified in peri-infarct area and its contralateral cortex. The rate of the positively stained area was compared between the two groups.

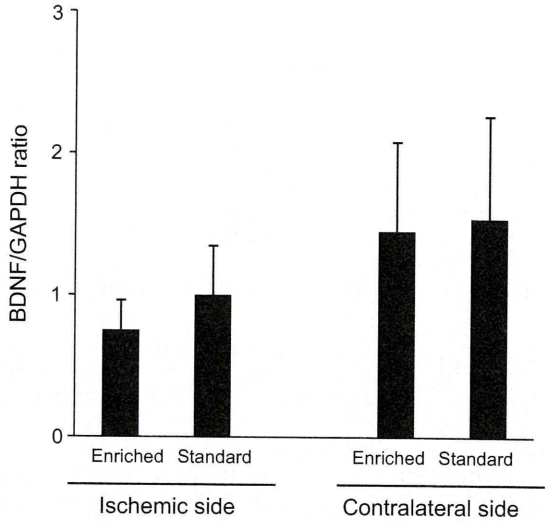


**Fig. 1.** BDNF gene expression showed no significant differences between the enriched and standard groups on the ischemic side ($p = 0.16$) or contralateral side ($p = 0.81$). Data were normalized to the ischemic side of the standard group.

The peri-infarct cortex and its contralateral cortex of the third blocks were subjected to real-time RT-PCR or Western blotting. Total RNA from the peri-infarct cortex and contralateral cortex was isolated and analyzed for gene expression by real-time quantitative RT-PCR. Expression levels of BDNF mRNA were normalized to those of GAPDH mRNA. For Western blotting, primary antibodies were HRP-conjugated anti-β actin antibody, anti-BDNF antibody, and anti-proBDNF antibody. The anti-proBDNF antibody was produced in a rabbit by intravenous injection of proBDNF-specific peptide. The secondary antibody was HRP-conjugated anti-rabbit goat IgG. The chemiluminescence agents were ECL or ECL+Plus (GE Healthcare). An LAS-4000miniEPUV (FUJIFILM) CCD camera was used to quantify the band intensity. As positive controls, recombinant human BDNF and C6 glioma cell lysate was applied for Western blotting.

Data are expressed as the means ± SD, and a $p$-value less than 0.05 was considered statistically significant. See the supplementary document for more information about the methods.

The neurological and motor functions of rats in both groups were impaired after t-MCAO and improved on day 14 (Table 1). A significant difference was observed in both NSS and IPT on day 14, but not on day 0, between the enriched ($n = 24$) and standard ($n = 22$) groups. The recovery rate for NSS and improvement index for IPT both indicated a significant improvement in function in the enriched group compared to the standard group.

The infarction area evaluated by immunoreactivity to MAP-2 in the enriched group (56.82 ± 7.31%, $n = 14$) was not significantly different from that in the standard group (55.44 ± 11.50%, $n = 13$, $p = 0.72$).

We performed real-time RT-PCR to examine the changes in BDNF levels (Fig. 1). The data presented were normalized to the ischemic side of the standard group. On the ischemic side, the BDNF/GAPDH ratio was 0.75 ± 0.21 ($n = 7$) in the enriched group, which was slightly but not significantly lower than that in the stan-

**Table 1**
Behavioral test results.

| | Pre-MCAO | | Day 0 | | Day 14 | |
|---|---|---|---|---|---|---|
| | Enriched $n=24$ | Standard $n=22$ | Enriched | Standard | Enriched | Standard |
| NSS | 0.00 ± 0.00 | 0.00 ± 0.00 | 8.00 ± 1.02 | 7.55 ± 0.74 | 4.92 ± 1.32* | 5.73 ± 1.03 |
| NSS recovery rate | | | | | 37.83 ± 17.95* | 23.67 ± 14.08 |
| IPT up-headed | 51.72 ± 2.00 | 50.80 ± 1.74 | 42.26 ± 2.61 | 43.52 ± 2.34 | 47.54 ± 1.63* | 45.37 ± 2.30 |
| IPT right-headed | 50.60 ± 2.86 | 50.79 ± 2.62 | 41.63 ± 2.62 | 42.80 ± 2.94 | 47.08 ± 2.11* | 45.61 ± 2.11 |
| IPT mean | 51.16 ± 2.16 | 50.79 ± 1.90 | 41.94 ± 2.39 | 43.16 ± 2.37 | 47.31 ± 1.70* | 45.49 ± 2.15 |
| IPT improvement index | | | | | 59.17 ± 29.51* | 27.75 ± 40.25 |

* $p<0.05$ compared to the standard group. Data are presented as the means ± SD.

dard group (1.00 ± 0.35, $n=6$). On the contralateral non-ischemic side, there was no significant difference in the BDNF/GAPDH ratio between the enriched group (1.45 ± 0.63, $n=8$) and standard group (1.54 ± 0.72, $n=6$).

Fig. 2 summarizes the results of Western blotting for matBDNF and proBDNF. The antibodies for matBDNF and proBDNF were validated with Western blotting using recombinant matBDNF and C6 glioma cell lysate, respectively (Fig. 2A). There were no significant differences between the enriched group ($n=8$) and standard group ($n=8$) in either matBDNF on the ischemic side (Fig. 2B), matBDNF on the contralateral side (Fig. 2C), proBDNF on the ischemic side (Fig. 2D), or proBDNF on the contralateral side (Fig. 2E), although the level of matBDNF in ischemic side tended to be slightly lower in the enriched group than in the contralateral group.

Fig. 3 shows the results of immunohistochemical staining of GFAP, SYP and BDNF. The areas stained with SYP and BDNF were quantified. The SYP-stained area on the ischemic side ($n=14$) was significantly increased in the enriched group ($n=13$) compared to the standard group (Fig. 3B, 2.57 ± 0.28% vs 2.07 ± 0.23%, $p<0.001$), although no significant difference was observed on the contralateral side (Fig. 3C, 1.56 ± 0.29% vs 1.49 ± 0.30%, $p=0.52$). On the other hand, the matBDNF-stained area on the ischemic side was slightly smaller in the enriched group ($n=15$) than in the standard group ($n=12$), although the difference did not reach the level of statistical significance (Fig. 3D). On the contralateral side, the enriched group showed a matBDNF-stained area comparable to that of the standard group without significant difference (Fig. 3E).

This study showed that housing in an enriched environment for 2 weeks significantly enhanced the functional recovery of rats after ischemic stroke. In addition, the immunohistochemical findings of increased SYP staining indicated an increased density of synapses. On the other hand, no significant difference was observed in the volume of infarction, mRNA expression of BDNF, or protein expressions of BDNFs.

Our previous investigation using a 4-week period of housing demonstrated a decrease in BDNF gene in the animals housed in an enriched environment based on microarray analysis and real-time RT-PCR as well as a continuous improvement of neurological functions until 4-week [16]. To further clarify the mechanisms of decreased BDNF expression, in the present study we measured the levels of the BDNF protein and gene after a shorter period of enriched environment, i.e., 2 weeks. The common finding between

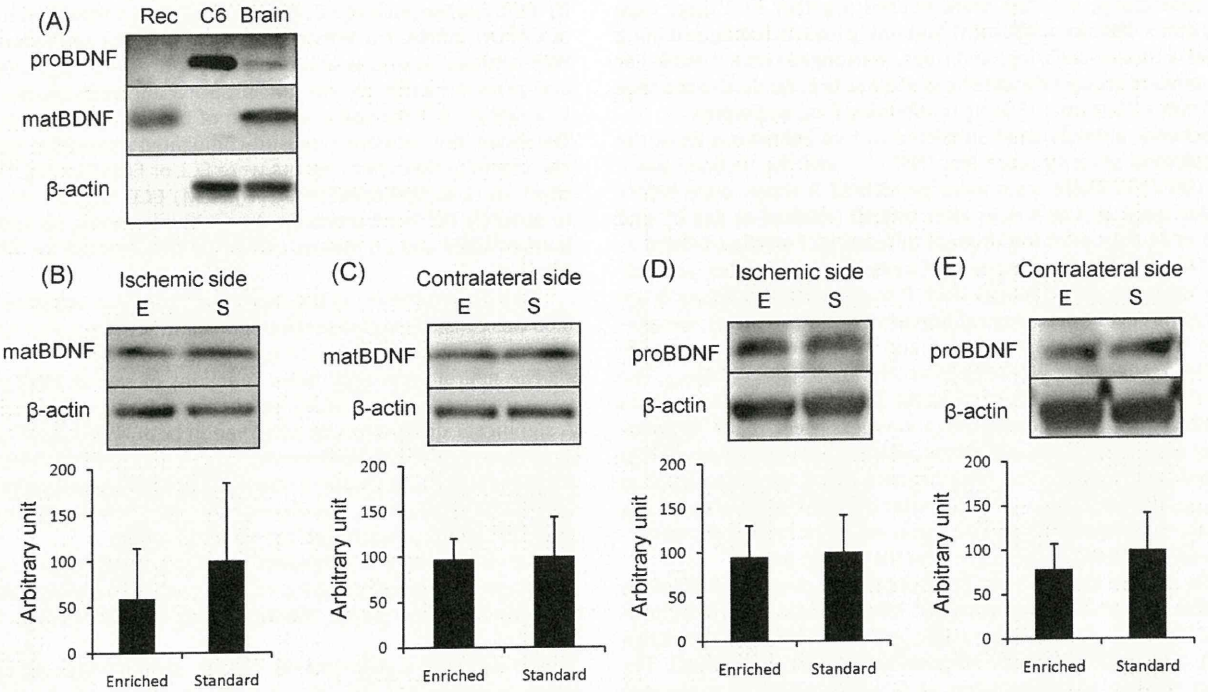


**Fig. 2.** Western blotting. (A) Recombinant human matBDNF (Rec), C6 glioma cell lysate (C6), and rat brain tissue validated the use of the antibodies for matBDNF (14 kDa) and proBDNF (32 kDa). Rat brain tissue contained detectable levels of these molecules. The levels of (B) matBDNF on the ischemic side ($p=0.27$), (C) matBDNF in contralateral side ($p=0.86$), (D) proBDNF on the ischemic side ($p=0.79$), and (E) proBDNF on the contralateral side ($p=0.25$) were not significantly different between the enriched and standard groups. Abbr. E: enriched group; S: standard group.

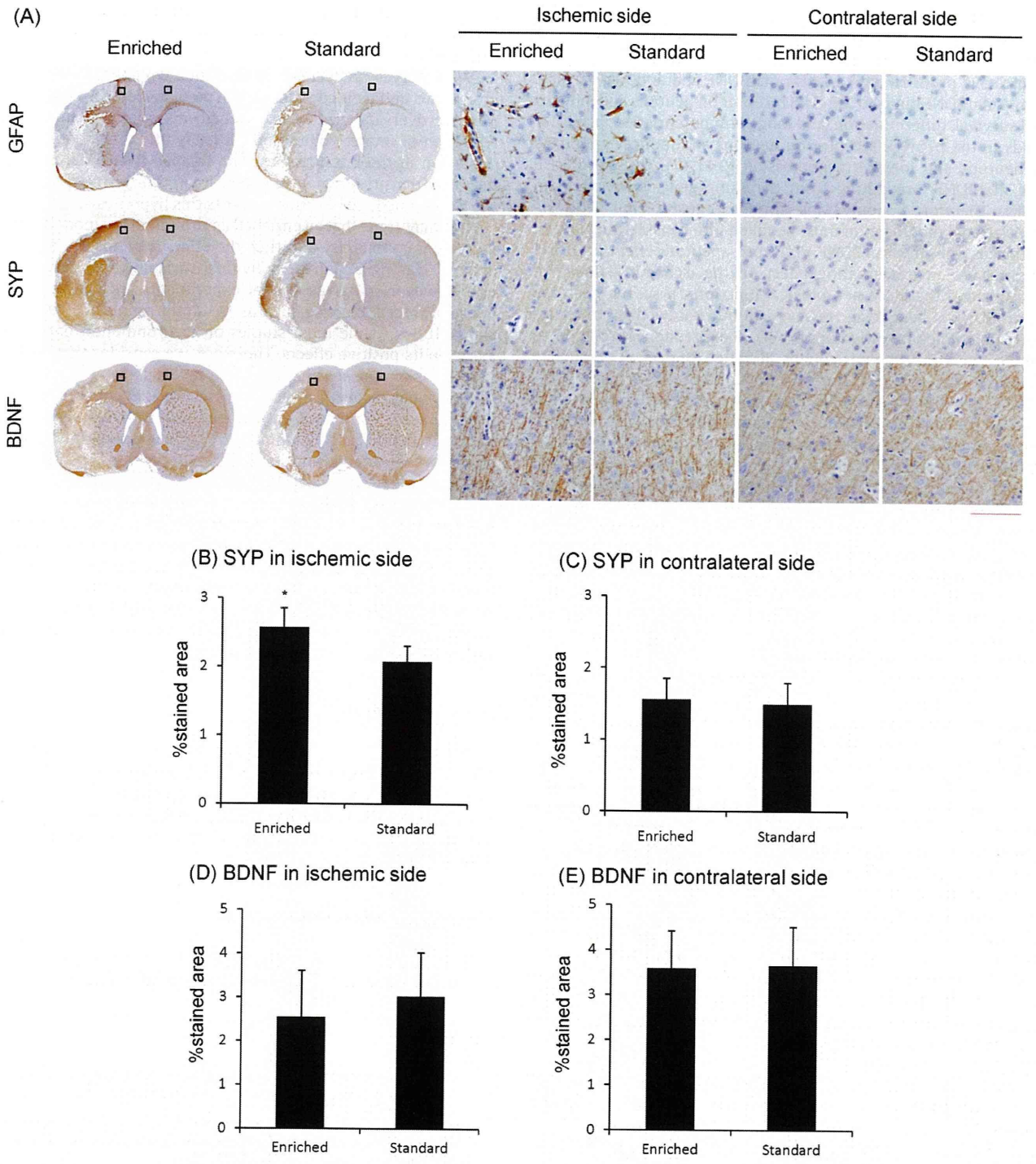


**Fig. 3.** Immunohistochemical analysis of GFAP, SYP, and matBDNF levels on the ischemic side and contralateral side. (A) Representative whole brain images (left 2 columns) and enlarged images (right 4 columns). The ischemic side was the left in the picture (right hemisphere of the rats). Squares indicate the enlarged sites. The bar represents 100 μm. (B–E) The SYP- and BDNF-stained areas were quantified. The ischemic side in the enriched group showed significantly stronger staining than the ischemic side in the standard group (B) ($p < 0.001$), while the contralateral side in the enriched group and contralateral side in the standard group did not show a significant difference (C) ($p = 0.52$). On the other hand, the matBDNF-stained area on the ischemic side (D) ($p = 0.24$) and contralateral side (E) ($p = 0.85$) showed no significant difference.

the 2-week and 4-week experiments was the lack of a clear increase in BDNF gene expression, despite the well-known beneficial effects of BDNF for neurons and neurological functions under various physiological and pathological conditions. These results, combined with our previous findings showing amelioration of neurological sign after 2 weeks, suggest that the functional recovery induced by an enriched environment might be brought about by mechanisms other than increased BDNF.

As an explanation for the relationship between BDNF and functional recovery, we hypothesized that proBDNF might play an

important role. The primary product of the BDNF gene is the 32-kDa proBDNF protein, which is translated in neurons and released into the extracellular space. Proteolytic enzymes such as plasmin cleave proBDNF into 14-kDa matBDNF and another particle. While matBDNF binds to the TrkB receptor on neurons and induces cell survival, differentiation, and long-term potentiation, proBDNF binds to the p75NTR receptor on neurons and induces apoptosis of neurons and long-term depression [9,11,17]. Thus, proBDNF and matBDNF, originating from the same gene, have opposite effects. Therefore, not only transcriptional regulation but also post-translational modification must be taken into consideration when we discuss the effects of BDNF. Via its pro-apoptotic effect, proBDNF might have an exacerbating effect on the ischemic damage of neurons and therefore neurological functions. If so, the decrease in proBDNF is beneficial. However, to our knowledge, there has been no studies investigating proBDNF expression in relation to stroke and enriched environment, although Zhao et al. previously measured the total levels of matBDNF and proBDNF using ELISA with anti-matBDNF antibody [20]. In the present work, we first tried to measure proBDNF using commercially available antibodies. Theoretically, Western blotting using either a proBDNF-specific antibody or matBDNF antibody could be used to quantify proBDNF levels, since the matBDNF domain is common to proBDNF and matBDNF. However, we did not find an efficient antibody that clearly revealed the band of proBDNF. Therefore, in the present study, we produced a polyclonal antibody using a proBDNF-specific peptide. Contrary to our expectations, Western blotting revealed no significant difference in proBDNF expression between the enriched group and standard group. This finding clearly indicates that the functional improvement induced by an enriched environment cannot be ascribed to decreased proBDNF.

On the other hand, an interesting difference between the 2-week and 4-week experiment is that a significant decrease in BDNF gene expression was observed after 4 weeks but not after 2 weeks of enrichment. Therefore, the difference in BDNF expression may be amplified between 2 weeks and 4 weeks. Considering that functional recovery and synaptogenesis were already observed at 2 weeks, there is a possibility that the decrease of BDNF expression at 4 weeks might result from secondary down-regulation due to the improved neurological functions. To prove the hypothesis, further investigation will be necessary to collect samples in earlier time points than 2 weeks, especially before the significant improvement becomes evident in enriched group. Not only BDNF gene expression but also matBDNF protein showed a consistent trend of decrease by both Western blotting and immunohistochemical staining, although the difference was not statistically significant. These results agree with the report by Zhao et al., which demonstrated a decrease in the total levels of BDNF protein in an enriched group [20]. Thus, we cannot completely rule out type-2 statistical error that small analyzing numbers concealed the possible decrease in BDNF genes or matBDNF in enriched group. Even if that is the case, however, there is no evidence of increase in BDNF genes or matBDNF.

Few genes are known to have a relationship to enriched housing environments. Dahlqvist et al. reported an alteration in the levels of nerve growth factor-induced gene A and glucocorticoid receptor following environmental enrichment in rats [4]. We previously found that animals in an enriched housing group showed a decrease in Early growth response-1 (Erg-1) mRNA [16], which is an inflammatory gene associated with exacerbation of neurological deficits after stroke [18]. To clarify the mechanisms of enriched environment-induced functional recovery, future investigations of neurotrophic factors other than BDNF (i.e., nerve growth factor, neurotrophin-3, and neurotrophin-4) and other inflammatory genes will be needed. Since the environmental stimulation involves a series of complicated processes through which many genes and proteins are expected to alter their expression, the combination of exhaustive analysis of the relevant genes and proteins will provide additional information.

We observed no decrease in infarction volume in the enriched group. This finding is consistent with previous reports [1,13]. Functional recovery induced by an enriched environment is not due to a reduction of infarct volume but possibly due to functional compensation in the brain tissues that escaped from infarction. The increased density of synapses in peri-infarct cortex measured using the SYP-stained area further supports this hypothesis.

One may argue that an enriched environment is a model enhancing voluntary exercise and thus the effect depends on individual activity, leading to a great individual variability in stroke recovery. However, as far as animal experiments are concerned, the effect of forced exercise such as treadmill running is controversial [7,10,14], while most studies on environmental enrichment agree on its positive effects. Therefore, we consider that enriched housing is a more feasible model to investigate the mechanisms of functional recovery after brain ischemia. Because it is established that environmental enrichment leads to an increase in BDNF in non-ischemic healthy animals [5], we compared only ischemic rats between enriched and standard environments according to the previous research designs [19,20].

In conclusion, an improvement of neurological functions was induced by an enriched environment accompanied with an increased density of synapses but without a reduction of infarct volume. The 2-week environmental enrichment did not significantly alter BDNF expression, including BDNF mRNA, matBDNF protein, or proBDNF protein. These results suggest that the functional recovery might not be due to increased BDNF or decreased proBDNF but rather to other underlying mechanisms.

## Acknowledgements

This study was partially supported by Special Coordination Funds for Promoting Science and Technology of the Ministry of Education, Culture, Sports, Science and Technology of the Japanese Government. This research was also partially supported by a Grant-in-Aid for General Scientific Research from the Japan Society for the Promotion of Science.

## Appendix A. Supplementary data

Supplementary data associated with this article can be found, in the online version, at doi:10.1016/j.neulet.2011.03.068.

## References

[1] J. Biernaskie, D. Corbett, Enriched rehabilitative training promotes improved forelimb motor function and enhanced dendritic growth after focal ischemic injury, J. Neurosci. 21 (2001) 5272–5280.
[2] J. Chen, Y. Li, L. Wang, Z. Zhang, D. Lu, M. Lu, M. Chopp, Therapeutic benefit of intravenous administration of bone marrow stromal cells after cerebral ischemia in rats, Stroke 32 (2001) 1005–1011.
[3] S.C. Cramer, Repairing the human brain after stroke. I. Mechanisms of spontaneous recovery, Ann. Neurol. 63 (2008) 272–287.
[4] P. Dahlqvist, L. Zhao, I.M. Johansson, B. Mattsson, B.B. Johansson, J.R. Seckl, T. Olsson, Environmental enrichment alters nerve growth factor-induced gene A and glucocorticoid receptor messenger RNA expression after middle cerebral artery occlusion in rats, Neuroscience 93 (1999) 527–535.
[5] B.R. Ickes, T.M. Pham, L.A. Sanders, D.S. Albeck, A.H. Mohammed, A.C. Granholm, Long-term environmental enrichment leads to regional increases in neurotrophin levels in rat brain, Exp. Neurol. 164 (2000) 45–52.
[6] B.B. Johansson, A.L. Ohlsson, Environment, social interaction, and physical activity as determinants of functional outcome after cerebral infarction in the rat, Exp. Neurol. 139 (1996) 322–327.
[7] M.W. Kim, M.S. Bang, T.R. Han, Y.J. Ko, B.W. Yoon, J.H. Kim, L.M. Kang, K.M. Lee, M.H. Kim, Exercise increased BDNF and trkB in the contralateral hemisphere of the ischemic rat brain, Brain Res. 1052 (2005) 16–21.